

# Magnetic fields in the Large-Scale Structure of the Universe

D. Ryu · D. R. G. Schleicher · R.  
A. Treumann · C. G. Tsagas · L. M.  
Widrow

Received: date / Accepted: date

**Abstract** Magnetic fields appear to be ubiquitous in astrophysical environments. Their existence in the intracluster medium is established through observations of synchrotron emission and Faraday rotation. On the other hand, the nature of magnetic fields outside of clusters, where observations are scarce and controversial, remains largely unknown. In this chapter, we review recent developments in our understanding of the nature and origin of intergalactic magnetic fields, and in particular, intercluster fields. A plausible scenario for the origin of galactic and intergalactic magnetic fields is for seed fields, created in the early universe, to be amplified by turbulent flows induced during the formation of the large scale structure. We present several mechanisms for the generation of seed fields both before and after recombination. We then discuss the evolution and role of magnetic fields during the formation of the first stars. We describe the turbulent amplification of seed fields during the formation of large scale structure and the nature of the magnetic fields that arise. Finally, we discuss implications of intergalactic magnetic fields.

**Keywords** Large-scale structure of the universe · Magnetic field · Turbulence

---

Dongsu Ryu  
Department of Astronomy and Space Science, Chungnam National University, Daejeon 305-764, Korea, E-mail: ryu@canopus.cnu.ac.kr

Dominik R. G. Schleicher  
Georg-August-Universität, Institut für Astrophysik, Friedrich-Hund-Platz 1, 37077 Göttingen, Germany, E-mail: dschleic@astro.physik.uni-goettingen.de

Rudolf A. Treumann  
ISSI, CH-3012 Bern, Hallerstrasse 6, Switzerland, E-mail: treumann@issibern.ch

Christos G. Tsagas  
Department of Physics, Aristotle University of Thessaloniki, Thessaloniki 54124, Greece, E-mail: tsagas@astro.auth.gr

Lawrence M. Widrow  
Department of Physics, Queen's University, Kingston, Ontario, K7L 3N6, Canada, E-mail: widrow@astro.queensu.ca

---

## 1 Introduction

In the highly successful  $\Lambda$ CDM cosmology, the large scale structure (LSS) forms through a process known as hierarchical clustering in which small-scale objects collapse first and merge to form systems of ever-increasing size. This scenario leads to a “cosmic web” of structure where galaxies reside mainly along filaments while galaxy clusters arise at the intersections of two or more filaments (see, e.g., Bond et al. 1996). Furthermore, a picture of a multi-phase intergalactic medium (IGM) has emerged. A hot phase, often referred to as the intracluster medium (ICM) because it is found inside and around clusters and groups of galaxies, has a temperature  $T > 10^7$  K and is observable via X-ray emission. The warm-hot intergalactic medium (WHIM) ( $10^5 < T < 10^7$  K) is found mainly in filaments of galaxies (Cen and Ostriker 1999, Kang et al. 2005). Gas in the IGM is heated by cosmological shocks which arise as objects in the hierarchy form. (Ryu et al. 2003, Pfrommer et al. 2006, Kang et al. 2007, Skillman et al. 2008, Vazza et al. 2009).

Magnetic fields are observed in galaxies of all types and in galaxy clusters. Moreover, there is some evidence that they permeate the filaments of the cosmic web. Various scenarios for the origin of galactic magnetic fields are discussed in Widrow et al. (2010) of this volume. The basic idea is that weak fields, generated either by an exotic early universe mechanism or some astrophysical process, are amplified to  $\mu$ G strength during galaxy formation and by dynamo action during the subsequent quiescent phase of galaxy evolution. Similarly, weak seed magnetic fields can be amplified into the intergalactic magnetic field (IGMF) by turbulent flow motions during the formation of the LSS through a process known as small-scale turbulence dynamo. In a turbulence dynamo, kinetic energy of the fluid is converted to magnetic energy through stretching, twisting, and folding of the field (see, e.g., Subramanian 1999, Cho and Vishniac 2000, Haugen et al. 2004a,b,c, Schekochihin et al. 2004, Brandenburg and Subramanian 2005, Cho et al. 2009, Brandenburg et al. 2010, of this volume). In addition, feedback from the black hole regions in active galactic nuclei (AGNs) can also contribute and amplify magnetic fields in the IGM.

This chapter will explore the structure formation-magnetic field connection. In particular, we will address two interrelated questions. First, can the structure formation itself generate new magnetic fields and amplify existing ones? Second, what role do magnetic fields play in structure formation and in other astrophysical processes? An outline of the chapter is as follows: In Section 2, we briefly review the observational evidence for magnetic fields in the clusters and filaments of the cosmic web. In Section 3, we describe various astrophysical mechanisms for the generation of seed magnetic fields, which would later be maintained and amplified within galaxies and clusters. In Section 4, we discuss the evolution and role of magnetic fields during the first star formation: their stabilization due to a non-zero ionization degree as well as their potential implication for star formation. We then describe how magnetic fields are amplified during structure formation in Section 5. We discuss the effects of magnetic fields on the propagation of cosmic rays in the IGM and also the Faraday rotation measure (RM) induced by magnetic

fields in Section 6. Section 7 presents something of a departure from the more phenomenological and astrophysical discussion as it provides a formal treatment of the evolution of density perturbations in the presence of magnetic fields. Finally, a brief summary follows in Section 8.

## 2 Observational Evidence for Magnetic Fields in Clusters and Filaments

The existence and strength of the IGMF has been deduced from observations of synchrotron emission and confirmed directly from observations of RM (see, e.g., Carilli and Taylor 2002, Govoni and Feretti 2004, for review). Synchrotron emission from a galaxy cluster was first discovered by Large et al. (1959) who surveyed the Coma cluster in the radio. Since then, it has been observed in numerous clusters, either as radio halos or as radio relics (see, e.g., Govoni and Feretti 2004, Cassano et al. 2008, and references therein). The diffuse radiation from radio halos is mostly unpolarized, and is thought to emerge from turbulent magnetic fields in the ICM. The radiation from radio relics is highly polarized and is believed to be emitted from shocked regions in the ICM. The strength of the magnetic field in radio halos is estimated to be  $\sim 1\mu\text{G}$ , while stronger fields are found radio relics. These estimates either assume equipartition (also known as the minimum energy argument) or incorporate measurements of inverse-Compton emission.

Observations of the IGMF based on Faraday rotation have also been done, though mostly for magnetic fields in the ICM (see Carilli and Taylor 2002, and references therein). An RM map of the Coma cluster, for example, reveals a field with a strength  $\sim \mu\text{G}$  and a coherence length of order  $\sim 10$  kpc (Kim et al. 1990). For Abell clusters, the typical RM is  $\sim 100 - 200$   $\text{rad m}^{-2}$  which indicates an average field strength of  $\sim 5-10 \mu\text{G}$  (Clarke et al. 2001, Clarke 2004). RM maps of clusters can be used to determine the power spectrum of turbulent magnetic fields in the ICM. For instance, a Kolmogorov-like spectrum with a bending at a few kpc scale is found in the cooled core region of the Hydra cluster (Vogt and Enßlin 2005), and spectra consistent with the Kolmogorov spectrum were reported in the wider ICM for the Abell 2382 cluster (Guidetti et al. 2008) and for the Coma cluster (Bonafede et al. 2010).

The nature of the IGMF in filaments, on the contrary, remains largely unknown, because the studies of synchrotron emission and RM outside clusters are still scarce and controversial. Although faint radio emission has been observed in the outskirts of clusters (see, e.g., Kim et al. 1989), there are no confirmed observations of synchrotron emission from filaments. Such measurements present a challenge for current facilities. As well, the removal of the galactic foreground is a non-trivial task (see, e.g., Brown et al. 2010). At present there is an upper limit of  $\sim 0.1 \mu\text{G}$  for the strength of the IGMF in filaments based on the observed limit of the RMs of background quasars (Ryu et al. 1998, Xu et al. 2006).

Recently, Neronov and Vovk (2010), Aleksić et al. (2010) reported a lower bound for the strength of the magnetic field in voids. Their claim, if true, is significant as it would represent the first evidence for magnetic fields in

such low-density regions and on such large scales. The basic idea is that an IGMF will deflect charged particles that arise in an electromagnetic cascade whose source is the very high energy  $\gamma$ -rays produced in an AGN. A non-observation of  $\gamma$ -ray secondaries coincident with VHE  $\gamma$ -rays, is then taken as evidence of magnetic deflection along the path from the source to the observer. Neronov and Vovk (2010) quote a lower bound of  $B \geq 3 \times 10^{-16}$  G based on observations by the Fermi and the High Energy Stereoscopic System (HESS) telescopes. A similar analysis was performed by Aleksić et al. (2010) using data from the MAGIC telescope though they are more cautious in presenting their conclusions and model dependencies. Note that Neronov and Vovk (2010) assume continuous emission of gamma-rays for  $10^6$  years, or longer which may not be realistic. If this assumption is relaxed, then one obtains a more conservative lower bound (Dermer et al. 2011).

The detection of the IGMF in filaments, if it exists, might be made with the next generation radio facilities. These facilities include the Square Kilometer Array (SKA), and upcoming SKA pathfinders, the Australian SKA Pathfinder (ASKAP) and the South African Karoo Array Telescope (MeerKAT), as well the Low Frequency Array (LOFAR) (see, e.g., papers in Carilli and Rawlings 2004).

For discussions on magnetic fields in the ICM and cluster outskirts, see Schekochihin et al. (2010) and Brüggén et al. (2010) of this volume.

### 3 Plasma Physics Mechanisms for Seed Fields

#### 3.1 Biermann battery

The Biermann battery is a promising mechanism for the creation of astrophysical magnetic fields. The mechanism arises in an ionized plasma whenever baroclinity exists, that is, when isodensity surfaces do not coincide with isobaric surfaces. This situation leads to an extra pressure gradient term in Ohm's law which drives currents. These currents, in turn, generate magnetic fields at a rate given by

$$\frac{d\mathbf{B}}{dt} \sim \frac{m_e c}{e} \frac{\nabla \rho_e \times \nabla p_e}{\rho_e^2}, \quad (1)$$

where  $\rho_e$  and  $p_e$  are the electron density and pressure, respectively (Biermann 1950). Though the mechanism was originally studied in the context of stars (Biermann 1950), it may arise during structure formation in cosmology whenever the electron pressure and density gradients are not aligned, as often occurs in shocks (Pudritz and Silk 1989, Kulsrud et al. 1997, Davies and Widrow 2000, Xu et al. 2008).

We note that vorticity,  $\boldsymbol{\omega}$ , is generated when the total pressure and density gradients are not aligned (baroclinity of flows – see Equation 23 below). In an ionized plasma, a simple order of magnitude estimate yields

$$B \sim \frac{m_p c}{e} \omega \simeq 3 \times 10^{-21} \left( \frac{\omega}{\text{km s}^{-1} \text{ kpc}^{-1}} \right) \text{ Gauss} . \quad (2)$$

Since the present-day vorticity in the IGM is of order  $\sim$  a few  $\text{km s}^{-1} \text{kpc}^{-1}$  (see Section 5.1 below), the seed fields from the Biermann battery will be rather small ( $\sim 10^{-20}$  G). However, vorticity, and hence seed fields, were almost certainly larger at early times. The following argument, based on dimensional analysis, suggests that for the objects which dominate the structure hierarchy at a given epoch the ratio of the vorticity to the Hubble parameter,  $H$ , is roughly constant and of order a few hundred. Once an object collapses,  $M \simeq v^2 R/G$  where  $M$ ,  $v$ , and  $R$  are the characteristic mass, velocity and size of the object. The spherical collapse model, which serves as a useful toy-model for structure formation in an expanding universe, predicts that the mean density within an object is a factor  $f_c \simeq 200$  times the critical density,  $\rho_c$ . Moreover, objects tend to follow the mass-size relation  $M \propto R^2$ . If we put all this together and use the fact that the critical density scales as the square of the Hubble parameter, we find that  $\omega \simeq 300H \propto (1+z)^{3/2}$ . Thus, we expect larger seed fields at early times. Similarly, the dynamical time for objects formed in the early universe is shorter than for objects today and hence the amplification of the magnetic fields by dynamo action will be more rapid. In short, the Biermann battery-dynamo amplification process may well operate at all stages of the structure-formation hierarchy.

Various alternatives have also been considered. For example, Lazarian (1992) considered a battery driven by electron diffusion. Subramanian et al. (1994) considered the Biermann effect during the epoch of reionization when ionization fronts sweep through the medium generating currents and magnetic fields. The fields are again fairly modest, but could be large enough to seed a dynamo which then amplifies them to an astrophysically interesting strength.

### 3.2 Thermal fluctuations

At finite temperatures, a plasma exhibits a finite (though possibly low) level of thermal fluctuations at all scales  $L = 2\pi/k$  and frequencies  $\omega$ . Differences in the thermal motions between the different charges generate micro-currents and hence electromagnetic fields which, on average, provide a noisy electromagnetic background. In the early universe, the gas is both hot and dilute. For example, the gas temperature is  $T \sim \text{eV}$  both at the recombination epoch and after reionization but before the formation of LSS. Therefore, the cosmic gas constitutes a classical plasma to which the classical fluctuation theory (Sitenko 1967) can be applied.

According to this theory, the power spectral density of magnetic field fluctuations  $\mathbf{b}$  at wavenumber  $\mathbf{k}$  and frequency  $\omega$  is obtained from the spatial correlation function of the fluctuating magnetic fields and is given by

$$\frac{\langle b_i b_j \rangle_{\mathbf{k}\omega}}{\sqrt{2\pi}} = \frac{\mu_0 T}{\omega} \left( \delta_{ij} - \frac{k_i k_j}{k^2} \right) \frac{n^2 \text{Im } \epsilon_{\perp}}{|n^2 - \epsilon_{\perp}|^2}. \quad (3)$$

Here, the fluctuating field is designated by lower case letters,  $i, j = 1, 2, 3$ ,  $n^2 = k^2 c^2 / \omega^2$  is the index of refraction and  $\epsilon_{\perp}(\omega, \mathbf{k})$  is the complex transverse

dielectric response function of the isotropic plasma. The latter, in (nonrelativistic) thermal equilibrium, is given by

$$\epsilon_{\perp}(\omega, \mathbf{k}) = 1 - \sum_{e,i} \frac{\omega_{e,i}^2}{2\omega k^2} \int \frac{\mathbf{v} \times (\mathbf{k} \times \mathbf{v}) F'_{0,e,i}(v)}{\mathbf{k} \cdot \mathbf{v} - \omega} dv^3, \quad (4)$$

where the sum is over negative ( $e$ ) and positive ( $i$ ) charges,  $\omega_{e,i}$ , the respective plasma frequencies, and  $F'_0 \equiv \partial F_0 / \partial \mathbf{v}$ , the derivative of the equilibrium distribution  $F_0$  which is assumed to be Maxwellian. The response function becomes

$$\epsilon_{\perp} = 1 - \frac{\omega_e^2}{\omega^2} \left[ \Phi(\varpi) + \frac{\hat{\theta}}{M} \Phi(M\varpi) - i\varpi\sqrt{\pi} \left( e^{-\varpi^2} + \frac{\hat{\theta}}{M} e^{-M^2\varpi^2} \right) \right]. \quad (5)$$

Here,  $M^2 \equiv (m_i/m_e)\hat{\theta}$ , and  $\Phi(\varpi) \approx 2\varpi^2 + \dots$  is the Gordeyev integral of  $\varpi = \sqrt{3/2}(\omega/kc_s)$  with  $c_s^2 = 3T_e/m_e$ , the square of the sound speed, and  $\hat{\theta} = T_e/T_i$ . Only at very large ion temperature  $T_i \gg T_e$  do the ions contribute to the imaginary part.

Seed fields for a turbulence dynamo arise from the zero frequency contribution,  $\varpi \rightarrow 0$  (index 0 in the following equation), which yields the magnetic power spectral density

$$\frac{\langle b_i b_j \rangle_{0k}}{\sqrt{2\pi}} \approx \frac{\mu_0 m_e c^2}{4\omega_e} \frac{\hat{\theta}^{1/2} k \lambda_e}{(k^2 \lambda_e^2 - m_e/m_i)^2} \simeq \frac{10^{-37}}{L_{\text{kpc}} N_{[\text{cm}^{-3}]}} \sqrt{T_{\text{eV}}} \frac{\text{V}^2 \text{s}^3}{\text{m}}, \quad (6)$$

where  $\hat{\theta} \equiv T_e/m_e c^2$  is the normalized temperature  $T_e$  and  $T_{\text{e[eV]}}$  is temperature in eV,  $\lambda_e = c/\omega_e \simeq 6/N^{1/2}$  is the electron inertial length,  $N$  is the number density, and  $N_{[\text{cm}^{-3}]}$  the density in  $\text{cm}^{-3}$ . To obtain the last equality we have ignored the term  $k^2 \lambda_e^2$  which is negligible on galactic and extragalactic scales. The magnetic spectral energy density thus grows linearly with wavenumber  $k$ , i.e. it decreases with the scale  $L$ .

For comparison, a  $B = 1 \mu\text{G}$  field has the spectral energy density  $\langle B_{1\mu\text{G}}^2 \rangle_{0k} \approx 4.3 \times 10^{-14} \text{ V}^2 \text{s}^3/\text{m}$ . Were we to have integrated over all frequencies  $\varpi$ , we would have obtained the equipartition between magnetic and electron thermal energy densities  $\langle b^2 \rangle_{\mathbf{k}} = 2\mu_0 T_e$  which holds in thermal equilibrium. Evidently, the thermal fluctuation level in Equation (6) is quite low. In order to obtain a  $B = 1\mu\text{G}$  field, the spectral energy density must be amplified by the large factor of  $\sim 5 \times 10^{23} L_{\text{kpc}} N_{[\text{cm}^{-3}]} / \sqrt{T_{\text{eV}}}$ .

### 3.3 Filamentation instability

Dynamos on galactic or cluster scales need seed fields on comparably large scales to get them started. Moreover, large-scale dynamos require turbulence and/or helicity which may not exist at adequate levels. Recently, the so-called filamentation (or Weibel) instability (Weibel 1959, Fried 1959) has been discussed as a generator of the IGMF (Gruzinov and Waxman 1999, Gruzinov 2001, Medvedev and Loeb 1999) and a possible alternative to dynamos on

galactic and extragalactic scales. The Weibel instability does require a strong departure of the plasma state from thermal equilibrium, which can be provided by fast beams on the plasma background (Achterberg and Wiersma 2007, Fried 1959, Sakai et al. 2004) or temperature anisotropies. The latter can be caused by pressure anisotropies (Weibel 1959, Treumann 2010), shock waves (Jaroschek et al. 2005, Nishikawa et al. 2009), or thin current sheets. Turbulence, if it exists in the early universe, leads to thin current sheets which can accelerate particles by second-order Fermi acceleration (Jaroschek et al. 2008, Jaroschek and Hoshino 2009), the local electric field which is generated in the current sheets, or by reconnection. Here, we discuss the possibility that the instability is driven by kinetic pressure/temperature anisotropies in the absence of magnetic field, as a mechanism to create seed fields.

Pressure and temperature anisotropies are probably superior to the beam for driving the instability for the simple reason that beams are highly unstable with respect to high-frequency plasma instabilities (Langmuir and Buneman modes). If the beams have velocity  $V_b$  and are current-compensated (i.e., the velocities of particles with different charges are the same) then the two-stream instability is excited with growth rate  $\gamma_{ts} \simeq \sqrt{3}(N_b/2N)^{1/3}\omega_e$ . Current-compensated beams arise in the symmetric counter-streaming configurations found in shocks. For the reasonable beam density  $N_b \sim 0.1N$  we find  $\gamma_{ts} \approx 0.6\omega_e \sim \text{few kHz}$  with a wavenumber is  $k_{ts} \sim \omega_e/V_b$ . If the beams are not current compensated, which is the case in turbulence where a multitude of thin current sheets is generated, then the Buneman instability is excited with growth rate  $\gamma_B \sim 0.03\omega_e \sim 10^2 \text{ Hz}$ , if the current velocity  $V_c = V_e - V_i > v_e$  exceeds the electron thermal speed  $v_e$ . Otherwise, for  $V_c < v_e$ , the ion sound will be excited with growth rate roughly  $\gamma_{ia} \sim \omega_{pi} \sim \text{few } 10^2 \text{ Hz}$ . All these instabilities grow very fast and readily deplete the beams/streams, heating the electron plasma in the direction of flow and thus causing the pressure or temperature anisotropy of electrons with higher temperature along the flow direction, i.e.  $\parallel$  to  $\mathbf{V}_c$ . If this is assumed to be the (readily achieved) final microscopic state, then the temperature anisotropy  $A = T_{e\parallel}/T_e - 1 > 0$  becomes unstable with respect to the Weibel thermally anisotropic mode. The temperature anisotropy corresponds to a pressure anisotropy  $P_e = N[T_e\mathbf{1} + (T_{e\parallel} - T_e)\mathbf{V}_c\mathbf{V}_c/V_c^2]$ . One should note that only the electrons, because of their large mobility, are important; the ions are much less active on these microscopic time scales and thus do not contribute.

In this thermally anisotropic case, the electrons obey a bi-Maxwellian equilibrium distribution function

$$f_e(v_{\perp}, v_{\parallel}) = \frac{(m_e/2\pi)^{3/2}}{T_e\sqrt{T_{e\parallel}}} \exp\left[-\frac{m_e v_{\perp}^2}{2T_e} - \frac{m_e v_{\parallel}^2}{2T_{e\parallel}}\right], \quad (7)$$

and the Weibel instability takes over with the linear electromagnetic dispersion relation  $n^2 = \epsilon_{\perp}$  and the transverse dielectric response function

$$\epsilon_{\perp} \equiv 1 - \frac{\omega_e^2}{\omega^2} \{1 - (A + 1)[1 + \zeta Z(\zeta)]\} - \frac{\omega_i^2}{\omega^2} = n^2. \quad (8)$$

Here,  $Z(\zeta)$  is the plasma dispersion function,  $\zeta = \omega/k_{\perp}v_e$ , and  $v_e = \sqrt{2T_e/m_e}$  is the electron thermal speed perpendicular to current. The Weibel instability

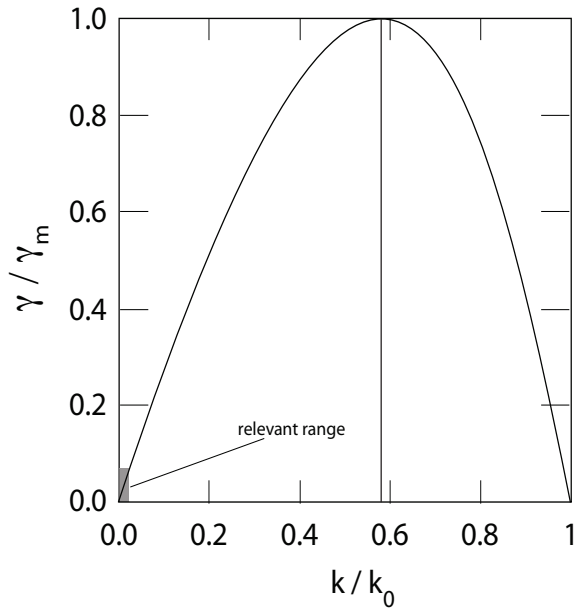


**Fig. 1** The growth rate  $\gamma = \gamma_W$  of the anisotropic-thermal Weibel instability normalized to the maximum growth,  $\gamma/\gamma_m$ , as a function of the normalized wavenumber  $k/k_0$  (see the text for the definition of  $k_0$ ). The vertical line indicates the position of the maximum growing wavenumber  $k_m/k_0 = 1/\sqrt{3}$ .

grows in the plane perpendicular to the direction of higher thermal velocity, which in our case has been assumed as the parallel direction. Hence,  $\mathbf{k} \equiv \mathbf{k}_\perp$ . The contribution of the resting ions has been retained for completeness; because of the smallness of the ion plasma frequency  $\omega_i \ll \omega_e$ , being much less than the electron plasma frequency  $\omega_e$ , it plays no role in the instability but is important in the discussion of the thermal level.

At zero real frequency,  $\omega = i\gamma$ , and the instability  $\gamma(k_\perp) > 0$  sets on for phase velocities  $\omega/k_\perp \ll v_e$  and wavenumbers  $k_\perp < k_0$  with growth rate

$$\frac{\gamma_W}{\omega_e} \simeq \sqrt{\frac{2}{\pi}} \frac{v_{e\perp}}{c} \frac{k_\perp}{k_0} \left(1 - \frac{k_\perp^2}{k_0^2}\right) (A+1)(k_0\lambda_e)^3, \quad (9)$$

vanishing at infinite wavelength  $k_\perp = 0$ , where  $k_0\lambda_e = \sqrt{A}$ . The growth rate maximizes at wavenumber  $k_m\lambda_e = k_0\lambda_e/\sqrt{3} = \sqrt{A/3}$  (see Figure 1), where its value is

$$\gamma_m \approx 34 \sqrt{N_{[\text{cm}^{-3}]} T_{e[\text{eV}]}} A^{3/2} (A+1) \text{ Hz}. \quad (10)$$

A substantial growth can be achieved and stationary (purely growing) non-fluctuating, short-wavelength magnetic fields are produced. The maximally growing wavelength is indeed very short. For a plasma density of  $N \approx 0.01 \text{ cm}^{-3}$ , the wavelength is only of the order of  $\lambda = (2\pi c/\omega_e)\sqrt{3/A} \sim 50\sqrt{3/A} \text{ km}$ . Even very weak anisotropies of  $A \sim 10^{-4}$  give  $\lambda_m \sim 10^4 \text{ km}$ . Galactic



or intergalactic scales  $L$  are far longer. For a realistic anisotropy of  $A \lesssim 1$ , at these large scales the growth rate scales with  $L$  as

$$\gamma_W \simeq 4A\sqrt{\pi\hat{\Theta}}(c/L) \simeq 10^{-13}A\sqrt{T_{\text{eV}}}/L_{\text{kpc}} \quad \text{Hz} \quad (11)$$

The above tells that mostly magnetic fields of small scales are excited and saturated by the instability, and those of galactic or intergalactic scales would not be substantial. Yet for  $A \sim 0.1$  and  $T \sim \text{eV}$ , the growth rate is  $\gamma_W \sim 10^{-14}$  Hz on kpc-scales which is quite large. Magnetic fields of  $\sim 10^{-16}$  G on kpc-scales would arise in  $\sim 10^7$  years or so provided the fields on smaller scales do not saturate the instability.

#### 4 Magnetic Fields after Recombination

If magnetic fields were created before or during recombination they could have had a significant impact on the thermal and chemical evolution of gas during the dark ages, on the formation of first stars and galaxies, and on the epoch of reionization (e.g., Sethi and Subramanian 2005, Tashiro and Sugiyama 2006, Sethi et al. 2008, Schleicher et al. 2008, 2009) (see also Widrow et al. 2010, of this volume). On the other hand, the first stars and galaxies may have been a source of magnetic fields. Our discussion should be viewed with a critical eye since the existence, strength and scale of early universe fields is highly uncertain (see e.g. Grasso and Rubinstein 2001) as is the efficiency of dynamo action at early times.

##### 4.1 Magnetic fields during the dark ages

The dark ages designate the period between recombination and reionization, during which no astronomical objects exist. The only radiation produced during this epoch is the 21 cm line of neutral hydrogen. The primordial gas consists of about 75% hydrogen and 25% helium, as well as traceable amounts of lithium and beryllium (both of the order  $10^{-9}$ ) (see, e.g., Kolb and Turner 1990). The ionization degree freezes out at about  $10^{-4}$  (Peebles 1968, Zeldovich et al. 1969, Seager et al. 1999). Though this ionization degree may seem rather low, it is significantly higher than the typical ionization degree in present-day molecular clouds (Myers and Khersonsky 1995). More to the point, it is high enough to prevent non-ideal magnetohydrodynamic (MHD) processes such as ambipolar or Ohmic diffusion from dissipating the magnetic fields.

The more relevant question is whether magnetic fields can be sustained during gravitational collapse when both the density and recombination rate increase and hence the ionization degree decreases. Gravitational collapse occurs on length scales where the thermal pressure can no longer balance the gravitational force. The critical length scale is given by the Jeans length

$$\lambda_J = \left( \frac{\pi c_s^2}{G\rho} \right)^{1/2}, \quad (12)$$

where  $c_s$  is the thermal sound speed and  $\rho$  the mass density. Previous studies by Maki and Susa (2004) and Glover and Savin (2009) followed the chemical evolution during gravitational collapse. Their one-zone model takes into account the density evolution in the central core, where the collapse takes place on the free-fall timescale  $t_{ff} \sim 1/\sqrt{G\rho}$ . As is well-known from analytic solutions and numerical simulations, the density in the central core is roughly homogeneous on the scale of the Jeans length  $\lambda_J$  (Larson 1969, Penston 1969, Abel et al. 2002, Bromm and Loeb 2003, Yoshida et al. 2008).

The calculations of Maki and Susa (2004) and Glover and Savin (2009) showed that the ionization degree evolves roughly as  $\rho^{-1/2}$  until a density of  $\sim 10^9 \text{ cm}^{-3}$  is reached. At this stage, the recombination rate becomes so high that the proton abundance becomes negligible. However, the presence of lithium and the low recombination rate of  $\text{Li}^+$  stabilizes the ionization degree at a level of  $\sim 10^{-10}$ , and it stays roughly constant even at higher densities.

In order to assess the implications of this result, Schleicher et al. (2009) combine the chemical network of Glover and Savin (2009) with a state-of-the-art model for ambipolar and Ohmic diffusions, based on the work of Pinto et al. (2008) and Pinto and Galli (2008). In their multi-fluid approach, the ambipolar diffusion rate is given as

$$L_{\text{AD}} = \frac{\eta_{\text{AD}}}{4\pi} |(\nabla \times \mathbf{B}) \times \mathbf{B}/B|^2, \quad (13)$$

where the  $\mathbf{B}$  denotes the magnetic field. The ambipolar diffusivity  $\eta_{\text{AD}}$  is given as

$$\eta_{\text{AD}}^{-1} = \sum_i \eta_{\text{AD},i}^{-1}, \quad (14)$$

with  $\eta_{\text{AD},i}$  denoting the ambipolar diffusivity due to an ionized species  $i$ . Similarly the Ohmic diffusion rate is given as

$$L_{\text{Ohm}} = \frac{\eta_{\text{O}}}{4\pi} |\nabla \times \mathbf{B}|^2, \quad (15)$$

with the Ohmic resistivity  $\eta_{\text{O}}$  given as

$$\eta_{\text{O}}^{-1} = \sum_i \eta_{\text{O},i}^{-1}. \quad (16)$$

The ambipolar resistivities  $\eta_{\text{AD},i}$  and the Ohmic resistivities  $\eta_{\text{O},i}$  due to ionized species  $i$  are calculated from the momentum-transfer coefficients as described in the appendix of Pinto et al. (2008).

To guide the physical intuition, we briefly summarize their results for the case of two charged fluids, e.g. electrons and positive ions, but note that the more detailed multi-fluid approach has been adopted in the calculations. The key quantities that regulate non-ideal MHD effects are the Hall parameters  $\beta_{\text{sn}}$ , defined as

$$\beta_{\text{sn}} = \left( \frac{q_s B}{m_s c} \right) \frac{m_s + m_n}{\rho_n \langle \sigma v \rangle_{\text{sn}}}. \quad (17)$$

Here,  $q_s$  denotes the charge of the species  $s$ ,  $m_s$  its mass,  $m_n$  the mass of the neutrals,  $\rho_n$  the neutral mass density,  $c$  the speed of light and  $\langle \sigma v \rangle_{\text{sn}}$  the

momentum-transfer coefficients between the ions and the neutrals (for the expressions, see Pinto and Galli (2008) and the discussion below). As shown by Pinto et al. (2008), the ambipolar and Ohmic resistivities are then given as

$$\eta_{\text{AD}} = \left( \frac{c^2}{4\pi\sigma} \right) \frac{\beta_{+n}|\beta_{-n}|}{\beta_{+n} + |\beta_{-n}|}, \quad (18)$$

$$\eta_{\text{O}} = \left( \frac{c^2}{4\pi\sigma} \right) \frac{1}{\beta_{+n} + |\beta_{-n}|}, \quad (19)$$

where  $\beta_{+n}, \beta_{-n}$  denote the Hall parameters for the positively and negatively charged species, and  $\sigma$  is given as

$$\sigma = \frac{q_+\rho_+c}{m_+B}. \quad (20)$$

In the latter expression,  $q_+$  denotes the positive charge, and  $\rho_+$  the mass density of the positively charged species.

For collisions involving protons and electrons, the momentum-transfer coefficients of Pinto and Galli (2008) are adopted. For collisions involving  $\text{Li}^+$ , the momentum-transfer coefficients using the polarization approximation are calculated, as described by Schleicher et al. (2009). This is indeed justified for collisions with helium (Cassidy and Elford 1985) and  $\text{H}_2$  (Dickinson et al. 1982, Røeggen et al. 2002). For collisions with atomic hydrogen, no detailed theoretical or experimental measurements are currently available. This process is of minor importance, however, as  $\text{Li}^+$  becomes the dominant ionized species at densities when molecular hydrogen is the dominant neutral species.

Equations (13) and (15) show that the dissipation rates depend on the magnetic field strength itself, and we note that also the ambipolar resistivities increase with increasing field strength (Pinto et al. 2008). During gravitational collapse, an initially weak field, for instance due to the Biermann battery (Xu et al. 2008), may be amplified both due to gravitational compression as well as turbulence dynamo (Schleicher et al. 2010). If the amplification due to turbulence dynamo is efficient, saturation may occur at equipartition or a somewhat lower level (see, e.g., Subramanian 1999, Cho and Vishniac 2000, Haugen et al. 2004a,b,c, Schekochihin et al. 2004, Brandenburg and Subramanian 2005, Cho et al. 2009). As ambipolar and Ohmic diffusions are stronger for stronger fields, we will initially focus on equipartition magnetic fields and show that magnetic fields can be sustained. The same is then true also for weaker magnetic fields.

To have a definite model, we assume Kolmogorov turbulence, and thus that the equipartition field strength scales as  $l^{1/3}$ . This is a good approximation for subsonic turbulence where compressional effects are of minor importance, and it is this type of turbulence that is expected in the first star-forming systems (Abel et al. 2002). The Ohmic and ambipolar diffusion scales are calculated as a function of the central core density and compared them to the Jeans length (see Figure 2). For clarity, the Ohmic / ambipolar diffusion scales are defined as the length scales on which the Ohmic or ambipolar diffusion time equals the eddy-turnover time. The calculation assumes that the turbulent velocity and the magnetic field follow a typical

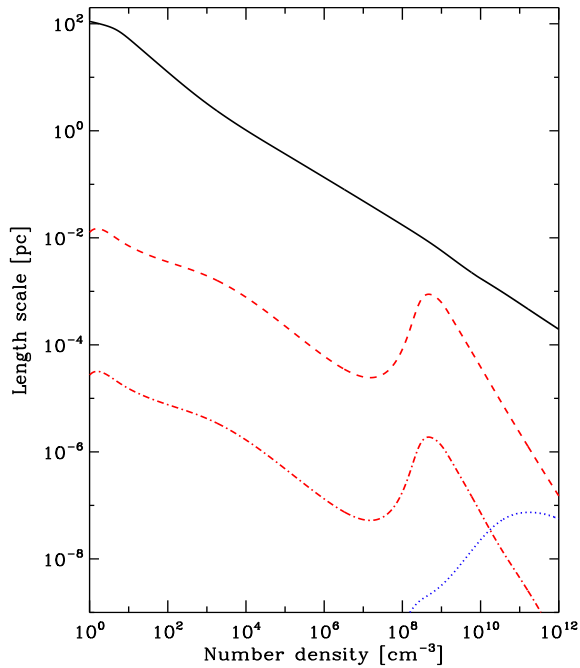


**Fig. 2** Diffusion length scales during gravitational collapse. The black solid line denotes the Jeans length as a function of central core density. The ambipolar diffusion scale for the equipartition magnetic field is given by the red dashed line, while the red dashed-dotted line corresponds to the scale for a weaker field (the magnetic energy equals 1/60 of the kinetic energy). The blue dotted line gives the Ohmic diffusion scale, which is independent of the magnetic field strength. In all cases, the dissipation scales are smaller than the Jeans length.

scaling law as expected for Kolmogorov turbulence. During collapse, the increased densities lead to a more efficient coupling between the ions and the neutrals, which largely compensates for the decreasing ionization degree. At a density of  $10^9 \text{ cm}^{-3}$ , the ambipolar diffusion scale increases due to a drop of the ionization degree at these high densities, but still stays an order of magnitude below the Jeans length. The Ohmic diffusion scale always stays orders of magnitude below the Jeans length. The figure also shows that when the magnetic field strength is below the equipartition value, the ambipolar diffusion scale is even small. The Ohmic dissipation scale, however, stays on the same low level, as the Ohmic dissipation rate scales roughly with the magnetic energy.

Numerical calculations suggest that the ionization degree may even be higher than expected from one-zone models, in particular due to the presence of shocks of Mach number  $\sim 1$  (Clark et al. 2011, Turk et al. 2009). So we safely conclude that during the dark ages, the magnetic fields up to the equipartition strength can be sustained even at high densities in collapsed regions.

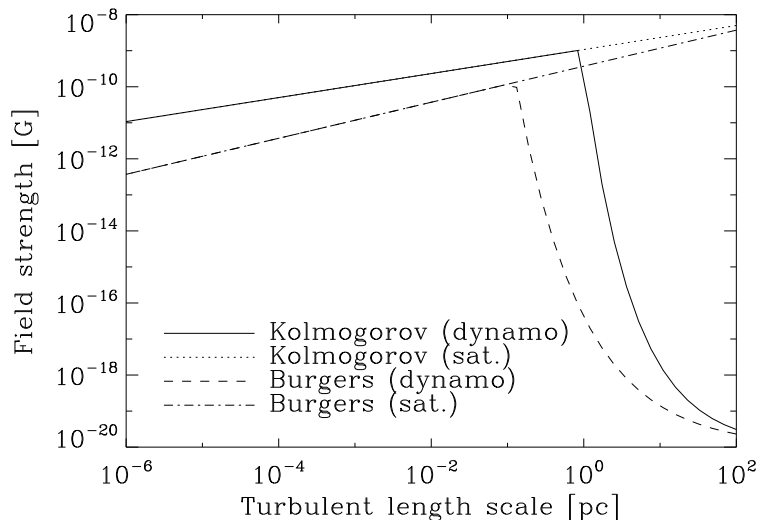


**Fig. 3** The magnetic field strength after a free-fall time. The horizontal axis denotes the length scale of the turbulent eddies. We assume a power-law scaling relation for the rms turbulence on a given length scale, and explore the cases of Kolmogorov and Burgers-type turbulence (Schleicher et al. 2010). In this model, the turbulent injection scale is 100 pc. For every length scale, we show both the maximum field strength that could be obtained from the small-scale dynamo, as well as our estimate for the actual field strength that might be produced within a free-fall time. The model suggests the production of strong magnetic fields on small scales.

#### 4.2 Magnetic field evolution in first star-forming halos

We now turn to the amplification of magnetic fields during the formation of the first stars. The halos that harbor the first stars at redshifts of  $z \sim 20 - 30$  typically have a total mass of  $10^6 M_{\odot}$ , consist of primordial gas with a temperature of  $\sim 3000$  K, and have a spatial extent of  $\sim 100$  pc. Turbulence is expected to be present, but on a subsonic level (Abel et al. 2002, Bromm and Loeb 2003, Yoshida et al. 2008). Such turbulence may create strong magnetic fields in the first galaxies and around them (Ryu et al. 2008, Arshakian et al. 2009, de Souza and Opher 2010, Schleicher et al. 2010).

Consider a simple model in which magnetic fields are amplified and saturate at a level corresponding to an energy 1/60 of the equipartition energy on an eddy turnover time  $t_{\text{eddy}}$ . We assume that turbulence is injected during the virialization phase on the length scale of the system (i.e.,  $\sim 100$  pc) with the velocity of the order of the sound speed. Both Kolmogorov and Burgers turbulences are considered; for Kolmogorov turbulence the velocity depends on the length scale as  $l^{1/3}$ , while for Burgers turbulence the scaling accords to  $l^{1/2}$ .

For magnetic fields to be relevant during the formation of the first stars, they must be amplified within the free-fall time scale  $t_{ff} \sim 1/\sqrt{G\rho}$ . The number of eddy turnovers is thus given by the ratio  $t_{ff}/t_{\text{eddy}}$ . Here, the eddy turnover time  $t_{\text{eddy}} \equiv l/v$  has a characteristic dependence on length

scale for Kolmogorov and Burgers turbulences. Then, the expected magnetic field strength is given in Figure 3 as a function of the length scale of turbulence. The preliminary calculation shows that magnetic fields of the order  $10^{-9}$  G can be reached in the first star-forming halos. For a comprehensive understanding of the strength and structure of the magnetic fields, the detailed implementation of turbulence dynamo will be required. Recent numerical MHD simulations suggest that the small-scale dynamo indeed operates during gravitational collapse, producing magnetic fields during the formation of the first structures (Sur et al. 2010, Federrath et al. 2011).

Additional amplification may occur after the formation of protostellar disks. In particular, a large-scale dynamo and the magneto-rotational instability may further enhance the magnetic fields in the first star-forming halos (Pudritz and Silk 1989, Tan and Blackman 2004, Silk and Langer 2006). For simplified field geometries, Machida et al. (2006, 2008) found that magnetic fields lead to the formation of jets and help to suppress fragmentation in protostellar disks. Fromang et al. (2004) studied self-gravitating magnetized disks and found that the interaction of turbulence created by the magneto-rotational instability may excite additional modes for the gravitational instability, and that the interaction of these modes reduces the accretion rate. This work suggests that magnetic fields may be amplified rapidly in the first star-forming halos and may become dynamically relevant though more realistic studies are necessary.

#### 4.3 Seed fields from astrophysical processes

The first stars probably possessed strong magnetic fields and therefore may have provided seed fields for dynamos in galaxies and in the IGM. If the stars subsequently explode as supernovae or lose a significant amount of mass through stellar winds, the fields ejected along with mass will find their way into the interstellar medium (ISM) and spread beyond galaxies into the IGM through galactic winds. Simple estimates by Syrovatskii (1970) illustrate the viability of the process. If there have been some  $10^8$  supernovae over the lifetime of galaxies, each of which spreads material through a  $(10 \text{ pc})^3$  volume. Using values for the field strength typical of the Crab nebula, one therefore expects galaxies to be filled by 10 pc regions with fields of strength  $\sim 3 \mu\text{G}$ . Assuming the same  $L^{-3/2}$  scaling, one finds fields of strength of  $\sim 10^{-11}$  G on 10 kpc scales. This value is significantly larger than those from the processes described in Section 3 and in Widrow et al. (2010) of this volume, although the filled volume is rather small. Recently, Donnert et al. (2009) suggested that galactic outflows during the starburst phase of galactic evolution can deposit a substantial amount of magnetic fields in the IGM.

Seed fields can be produced at cosmological shocks which were induced during the formation of the LSS of the universe (Ryu et al. 2003, Pfrommer et al. 2006, Kang et al. 2007, Skillman et al. 2008, Vazza et al. 2009) (see Section 5.1 for further description of cosmological shocks). Cosmological shocks are collisionless like shocks in other astrophysical environments, where CRs are accelerated at the same time as the gas is heated. During the process of acceleration, it was shown that the upstream magnetic field can be amplified

nonlinearly by non-resonant growing modes (Bell 2004). Then, the magnetic field can have the energy up to

$$\varepsilon_B \sim \frac{1}{2} \frac{U_{n1}}{c} \varepsilon_{\text{CRs}}. \quad (21)$$

With  $U_{n1}/c \sim 10^{-3}$  and Mach number a few in cosmological shocks (Ryu et al. 2003, Kang et al. 2007), we get  $\varepsilon_B \sim \varepsilon_{\text{CRs}} \sim \varepsilon_{\text{therm}}$ . In addition, the Weibel instability described in Section 3.3 can operate and produce magnetic fields up to the level of  $\varepsilon_B \sim 10^{-3} \varepsilon_{\text{sh}}$  (Schlickeiser and Shukla 2003, Medvedev et al. 2006). Here,  $\varepsilon_{\text{sh}}$  is the energy density of upstream flow, and  $\varepsilon_B$ ,  $\varepsilon_{\text{CRs}}$ , and  $\varepsilon_{\text{therm}}$  are the energy densities of downstream magnetic fields, CRs, and gas random motion, respectively. These processes can potentially produce strong fields around cosmological shocks, although the volume filling is small and the coherence length of the resulting fields is expected to be microscopic.

Other mechanisms have been proposed. For instance, recently, Miniati and Bell (2011) suggested that the return current which is induced by cosmic-rays produced by early supernovae can deposit seed fields into the IGM.

## 5 Magnetic Fields in the IGM

With the processes described in Sections 3 and 4 and also in Widrow et al. (2010) of this volume, there is no shortage of mechanisms to generate seed fields for the IGMF. Those fields are expected to be amplified by the turbulent flow motions which were induced during the formation of the LSS of the universe. The turbulence dynamo not only increases the strength of magnetic fields, but also produces the magnetic fields of large scales, up to the energy injection scale, through the inverse cascade. The beauty of the turbulence dynamo in LSS is that it erases the memory of weak seed fields and produces the IGMF, independent of the origin of seed fields.

### 5.1 Turbulence in the LSS of the universe

Signatures of turbulence have been observed in the ICM. For example, Schuecker et al. (2004) analyzed gas pressure maps that were constructed from XMM-Newton X-ray data. They claimed that in the Coma cluster, which appears to be in a post-merger state, pressure fluctuations are consistent with Kolmogorov turbulence. The turbulence is likely subsonic but with an energy that is at least 10 % of the thermal energy, i.e.,  $\varepsilon_{\text{turb}} > 0.1 \varepsilon_{\text{therm}}$ . The results agree with predictions from numerical simulations, namely that the flows in cluster scales have a power spectrum expected for Kolmogorov turbulence (Kulsrud et al. 1997, Kulsrud and Zweibel 2008), and even in relaxed clusters the flow motions have  $\varepsilon_{\text{kin}} \sim 0.1 \varepsilon_{\text{therm}}$  (Nagai et al. 2007). Turbulence in the ICM was also studied in RM maps of a few clusters (Vogt and Enßlin 2005, Guidetti et al. 2008, Bonafede et al. 2010).

Recently, Ryu et al. (2008) proposed a scenario in which vorticity is generated directly or indirectly at cosmological shocks and turbulence in the IGM

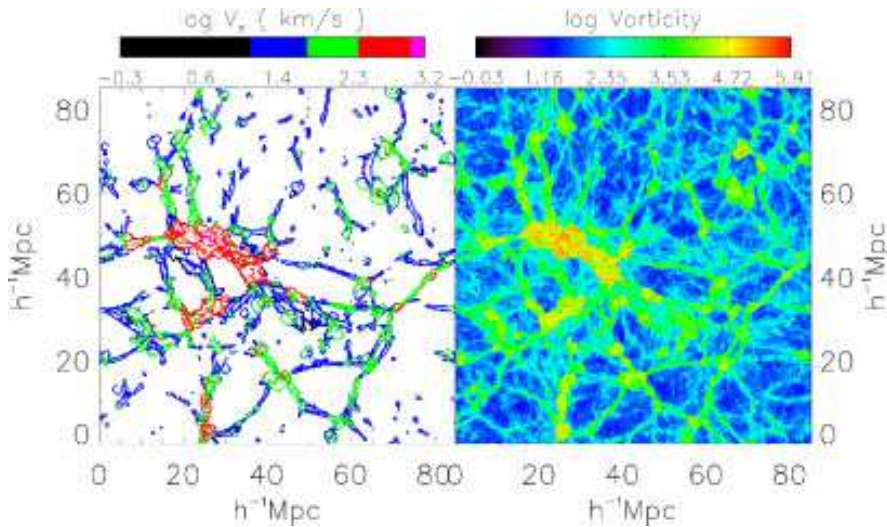


**Fig. 4** Two-dimensional slice of  $(85 h^{-1} \text{Mpc})^2$  showing shock locations with color-coded shock speed (left panel) and the magnitude of vorticity (right panel) at  $z = 0$ . The vorticity is given in units of  $10^{-4} t_{\text{age}}^{-1}$ , where  $t_{\text{age}}$  is the age of the universe.

is induced via the cascade of the vorticity. Here, we provide an estimate estimate of the turbulence seen in simulations for the formation of the LSS. The results are based on a simulation described in Cen and Ostriker (2006) which includes the radiative processes of heating/cooling and feedback from galactic superwind. The work of Ryu et al. (2008) utilized a simulation, where only the gravitational and gas dynamical processes are included.

In the simulation of Cen and Ostriker (2006), the WMAP1-normalized  $\Lambda$ CDM cosmology was employed with the following parameters:  $\Omega_b = 0.048$ ,  $\Omega_m = 0.31$ ,  $\Omega_\Lambda = 0.69$ ,  $h \equiv H_0/(100 \text{ km/s/Mpc}) = 0.69$ ,  $\sigma_8 = 0.89$ , and  $n = 0.97$ . A cubic box of comoving size  $85 h^{-1} \text{Mpc}$  was simulated using  $1024^3$  grid zones for gas and gravity and  $512^3$  particles for dark matter. It allows a uniform spatial resolution of  $\Delta l = 83 h^{-1} \text{kpc}$ . For detailed descriptions of input physics ingredients such as non-equilibrium ionization/cooling, photoionization/heating, star formation, and feedback processes, refer Cen et al. (2003) and Cen and Ostriker (2006). Feedback from star formation was treated in three forms: ionizing UV photons, galactic superwinds, and metal enrichment. Galactic superwinds were meant to represent cumulative supernova explosions, and modeled as outflows of several hundred  $\text{km s}^{-1}$ . The input of galactic superwind energy for a given amount of star formation was determined by matching the outflow velocities computed for star-burst galaxies in the simulation with those observed in the real world. The simulations were performed using a PM/Eulerian hydrodynamic cosmology code (Ryu et al. 1993).

In the IGM, vorticity,  $\boldsymbol{\omega} \equiv \nabla \times \mathbf{v}$ , can be generated directly at curved shocks and also by the baroclinity of flows. For uniform upstream flow, the



vorticity produced behind curved shock surface is

$$\boldsymbol{\omega}_{\text{cs}} = \frac{(\rho_2 - \rho_1)^2}{\rho_1 \rho_2} K \mathbf{U}_1 \times \hat{n}, \quad (22)$$

where  $\rho_1$  and  $\rho_2$  are the upstream and downstream gas densities, respectively,  $\mathbf{U}_1$  is the upstream flow velocity in the shock rest frame,  $K$  is the curvature tensor of the shock surface, and  $\hat{n}$  is the unit vector normal to the surface. If isopycnic surfaces do not coincide with isobaric surfaces, vorticity is generated with the rate given by

$$\dot{\boldsymbol{\omega}}_{\text{bc}} = \frac{1}{\rho^2} \nabla \rho \times \nabla p. \quad (23)$$

Shock waves are ubiquitous in the IGM, as in other astrophysical environments. The spatial distribution and properties of cosmological shocks in the LSS of the universe have been studied quantitatively using simulations for the formation of LSS (Ryu et al. 2003, Pfrommer et al. 2006, Kang et al. 2007, Skillman et al. 2008, Vazza et al. 2009). In the cold dark matter universe with cosmological constant ( $\Lambda$ CDM), shocks with Mach number up to a few hundreds and speed up to a couple of thousand  $\text{km s}^{-1}$  are present at the present universe ( $z = 0$ ). In the left panel of Figure 4, the spatial distribution of cosmological shocks is shown. Numerous shocks are found. External shocks exist around sheets, filaments, and knots of mass distribution, which form when the gas in void regions accretes onto them. Within those nonlinear structures, internal shocks exist, which form by infall of previously shocked gas to filaments and knots, and during subclump mergers, as well as by chaotic flow motions. Due to the low temperature of the accreting gas, the Mach number of external shocks is high, extending up to  $M \sim$  a few  $\times 100$ , while internal shocks have mostly low Mach number of  $M \sim$  a few. The mean distance between shock surfaces is  $\sim 3 h^{-1} \text{Mpc}$  when averaged over all the universe, or  $\sim 1 h^{-1} \text{Mpc}$  inside nonlinear structures. Internal shocks of  $M \sim 2 - 4$  formed with hot and high-density gas are responsible for most of shock dissipation into heat and CRs. It was shown that the shock dissipation can count most of the gas thermal energy in the IGM (Kang et al. 2005).

In the right panel of Figure 4, the distribution of vorticity is shown. It closely matches that of shocks, suggesting that a substantial portion of the vorticity, if not all, has been generated at the shocks. As a matter of fact, as was noted in Ryu et al. (2008), the vorticity in the IGM can be accounted with that generated either directly at curved cosmological shocks or by the baroclinity of flows. The contributions from the two processes are comparable. The baroclinity resulted from the entropy variation induced at shocks. So all the vorticity generation also can be attributed to the presence of cosmological shocks.

For quantification of vorticity, the flow velocity is decomposed into

$$\mathbf{v} = \mathbf{v}_{\text{div}} + \mathbf{v}_{\text{curl}} + \mathbf{v}_{\text{unif}}, \quad (24)$$

where the divergence and curl components are defined as  $\nabla \cdot \mathbf{v}_{\text{div}} \equiv \nabla \cdot \mathbf{v}$  and  $\nabla \times \mathbf{v}_{\text{curl}} \equiv \nabla \times \mathbf{v}$ , respectively. That is,  $\mathbf{v}_{\text{div}}$  is associated to compressional motions, while  $\mathbf{v}_{\text{curl}}$  to incompressible shear motions. Here  $\mathbf{v}_{\text{unif}}$  is the

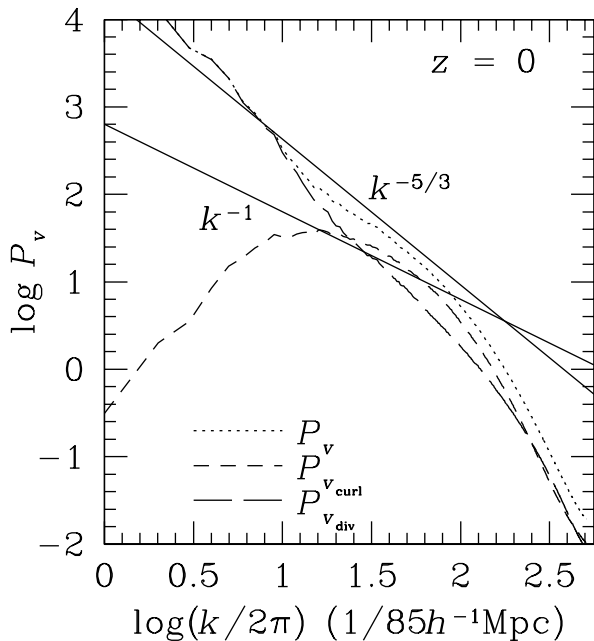


**Fig. 5** Power spectra,  $\int P_v dk = \langle (1/2)v^2 \rangle$ , for the gas velocity and its curl and divergence components at  $z = 0$ . Two straight lines of slopes  $-5/3$  and  $-1$  are also drawn for comparison.

component uniform across the computational box, whose magnitude is much smaller than the other two components. The decomposition is calculated exactly in Fourier space. We note with the above decomposition, locally

$$\mathbf{v}_{\text{div}} \cdot \mathbf{v}_{\text{curl}} \neq 0 \quad \text{so} \quad \frac{1}{2}v^2 \neq \frac{1}{2}(v_{\text{div}}^2 + v_{\text{curl}}^2). \quad (25)$$

However, globally

$$\int_{\text{box}} \mathbf{v}_{\text{div}} \cdot \mathbf{v}_{\text{curl}} d^3\mathbf{x} = 0 \quad \text{so} \quad \int_{\text{box}} \frac{1}{2}v^2 d^3\mathbf{x} = \int_{\text{box}} \frac{1}{2}(v_{\text{div}}^2 + v_{\text{curl}}^2) d^3\mathbf{x}. \quad (26)$$

The power spectra for the gas velocity and its curl and divergence components at the present universe are shown in Figure 5. At long wavelengths, the amplitude of perturbations are small, so that linear theory applies. That is,  $P_{\text{curl}}(k) \rightarrow 0$  as  $k \rightarrow 0$ , while  $P_{\text{div}}(k)$  follows the analytic theory expectation,  $P_{\text{div}}(k) \sim k^{-1}$ . For wavelengths smaller than a few Mpc, nonlinearities dominate, and we see  $P_{\text{curl}}(k) \gtrsim P_{\text{div}}(k)$ .  $P_{\text{curl}}(k)$  peaks at  $\sim 5 h^{-1}$  Mpc, and for  $k$  somewhat larger than the peak wavenumber, the spectrum follows a power law of  $k^{-5/3}$ , the Kolmogorov spectrum.  $P_{\text{curl}}(k)$  has most power at  $\sim 2 - 3 h^{-1}$  Mpc, that indicates the typical scale of nonlinear structures in the simulation.

The vorticity in the IGM as a function of gas density and temperature is shown in the left panel of Figure 6. The figure exhibits a clear trend

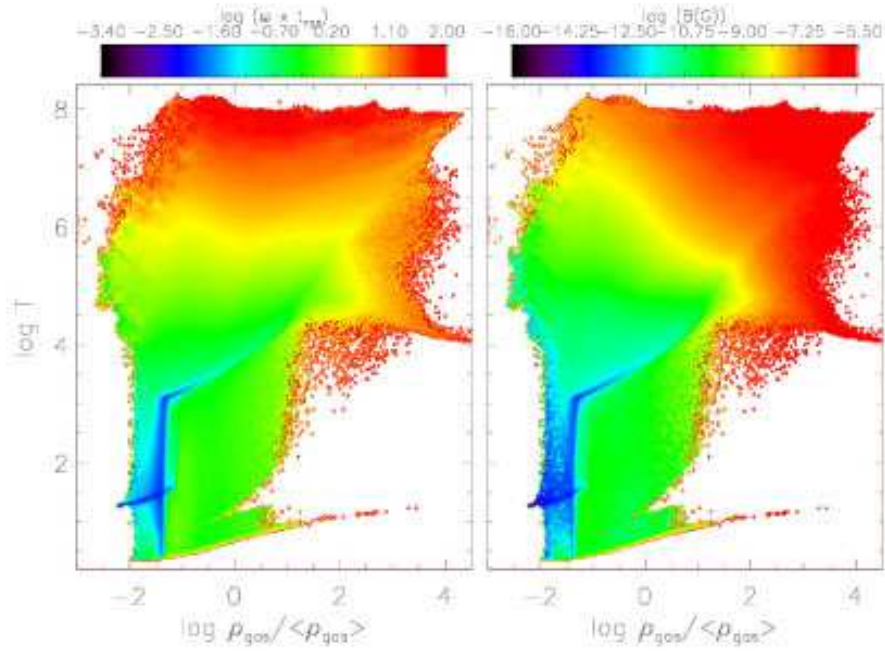


**Fig. 6** Distribution of the magnitude of the vorticity in the IGM (left panel) and the strength of the IGMF (right panel) in the density-temperature plane at  $z = 0$ . The vorticity is given in units of  $t_{\text{age}}^{-1}$ .

that the vorticity is larger in hotter regions. It is because hotter regions are occupied with the gas that has gone through shocks of larger speed. The vorticity generated at shocks of larger speed should be on average larger. Also, there are regions of high density ( $\rho_{\text{gas}}/\langle\rho_{\text{gas}}\rangle \lesssim 100$ ) and warm temperature ( $T \gtrsim 10^4$  K), where the vorticity is large. These regions contain the gas that was heated to high temperature and subsequently cooled down.

In the left panel of Figure 7, the root-meas-square (rms) of the vorticity at a few redshifts for the gas in the four phases of the IGM is shown. Note that the vorticity shown was computed over the same comoving scales, and normalized with the age of the universe at given  $z$ . The vorticity increases as the universe evolves and the LSS of the universe develops. But over the period of the time presented in the figure, the vorticity, especially in the hot IGM and WHIM, has increased just by a factor of a few.

Figures 6 and 7 indicate that at the present epoch,  $\omega_{\text{rms}}t_{\text{age}} \sim$  a few  $\times 10$  inside and around clusters/groups with  $T \gtrsim 10^7$  K and  $\sim 10$  in filaments which is filled mostly with the WHIM. On the other hand,  $\omega_{\text{rms}}t_{\text{age}}$  is on the order of unity in sheetlike structures and even smaller in voids. Here,  $t_{\text{age}}$  is the present age of the universe, so  $\omega_{\text{rms}}t_{\text{age}}$  represents the number of eddy turnovers in the age of the universe. It takes a few turnover times for vorticity to decay and develop into turbulence. So it is likely that the flows in clusters/groups and filaments is in a turbulent state, while turbulence have not significantly developed in sheetlike structures and voids.

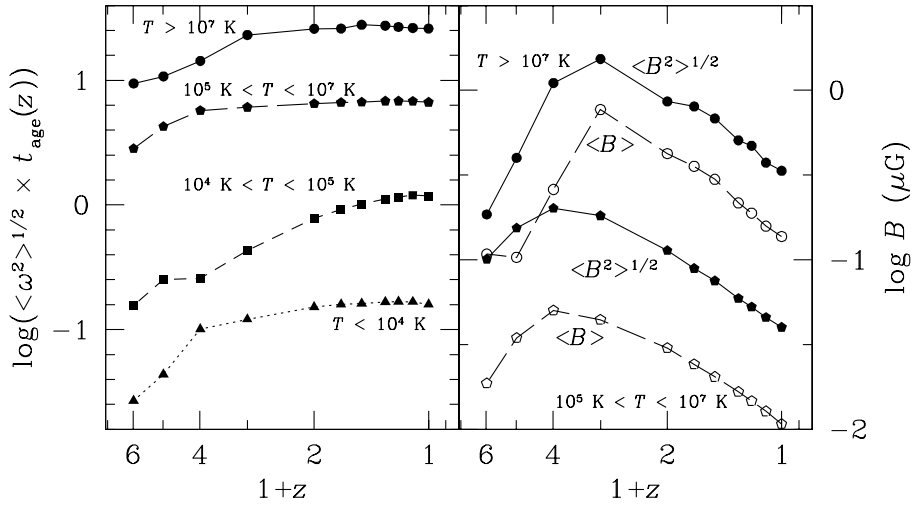


**Fig. 7** The time evolution of the rms of the vorticity for four temperature phases of the IGM (left panel) and the time evolution of the averaged strengths of the IGMF for the hot IGM and WHIM (right panel) as a function of redshift  $z$ . The vorticity is given in units of  $t_{\text{age}}(z)^{-1}$ , where  $t_{\text{age}}(z)$  is the age of the universe at  $z$ .

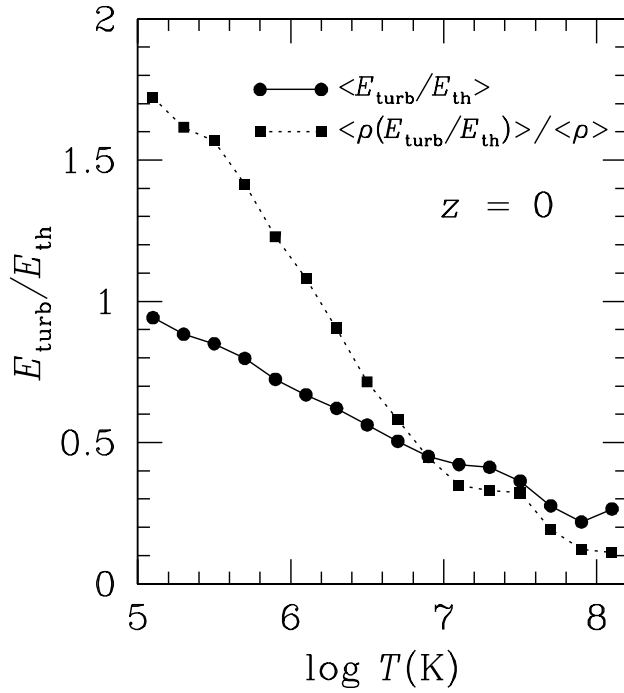


**Fig. 8** Turbulence to thermal energy ratio as a function of temperature at  $z = 0$ . The values shown are volume-averaged and mass-averaged over temperature bins.

To estimate the energy associated with the turbulence induced in the IGM via the cascade of the vorticity, we assume that the energy of vortical motions,  $(1/2)\rho_{\text{gas}}v_{\text{curl}}^2$ , is transferred to that of turbulent motions. Then, we can regard it as the turbulence energy,  $\varepsilon_{\text{turb}}$ . Figure 8 shows the ratio of the turbulence to thermal energies in clusters/groups and filaments as a function of temperature at the present universe. In clusters/groups with  $T \gtrsim 10^7$  K,  $\varepsilon_{\text{turb}} < \varepsilon_{\text{therm}}$ . Particularly the mass averaged value shows that  $\varepsilon_{\text{turb}}/\varepsilon_{\text{therm}}$  would be  $\sim 0.1 - 0.3$  in cluster cores. The predicted  $\varepsilon_{\text{turb}}/\varepsilon_{\text{therm}}$  is in a good agreement with observation (Schuecker et al. 2004). Note that  $M_{\text{turb}} \equiv v_{\text{curl}}/c_s = \sqrt{1.8} (\varepsilon_{\text{turb}}/\varepsilon_{\text{therm}})^{1/2}$ , where  $c_s$  is the sound speed. Therefore, overall turbulence is subsonic in clusters/groups, whereas it is transonic or mildly supersonic in filaments.

## 5.2 Amplification of the IGMF by the turbulence in the IGM

In principle, if simulations for the formation of LSS in the universe includes magnetic fields, that is, if they are MHD, the amplification of the seed magnetic fields by the turbulent motions in the IGM should be able to be followed. But, in reality, simulations with the current capacity of computing power have too low a resolution to reproduce the full development of turbulence inside nonlinear structures. Also the numerical resistivity is larger than the physical resistivity by great many order of magnitude. As a result, the growth of magnetic fields is saturated before dynamo action become fully operative, and the amplification of magnetic fields can not be followed correctly, as was already pointed in (Kulsrud et al. 1997).

In order to reproduce the growth of magnetic fields by dynamo action, a separate three-dimensional simulation of MHD turbulence in a controlled box was performed; incompressible, driven turbulence with initially very weak or zero magnetic fields was simulated using a pseudospectral code (Cho and Vishniac 2000). Hyperviscosity and hyperresistivity with the Prandtl number of unity were used. The advantage of performing incompressible simulations using a pseudospectral code is that the intrinsic numerical viscosity and resistivity are virtually zero. And by using hyperviscosity and hyperresistivity, the inertial range can be maximized. We point that it would take much higher resolution to achieve the same growth rate in simulations of compressible MHD turbulence.

The top-left panel of Figure 9 shows the time evolution of kinetic and magnetic energies for four different simulations: 256H8-B<sub>0</sub>10<sup>-3</sup>, 256H3-B<sub>0</sub>10<sup>-3</sup>, 256H8-B<sub>0</sub>0, and 256H8-B<sub>0</sub>10<sup>-6</sup>. Simulations are denoted with 256Y-B<sub>0</sub>Z, where 256 refers to the number of grid points in each spatial direction, Y refers to hyperdissipation (H) and its order, and Z refers to the strength of the external magnetic fields. The turbulence was driven at the scale of  $L_0 \sim (1/2)L_{\text{box}}$  where  $L_{\text{box}}$  is the computational box size, and the driving strength was set so that the total energy is  $E_{\text{tot}} \equiv E_{\text{kin}} + E_B \sim 1$  at saturation. The time is given in units of the eddy turnover time that is defined as the inverse of vorticity at driving scale,  $t_{\text{eddy}} \equiv 1/\omega_{\text{driving}}$ , at saturation. See Cho et al. (2009) for details of simulations.

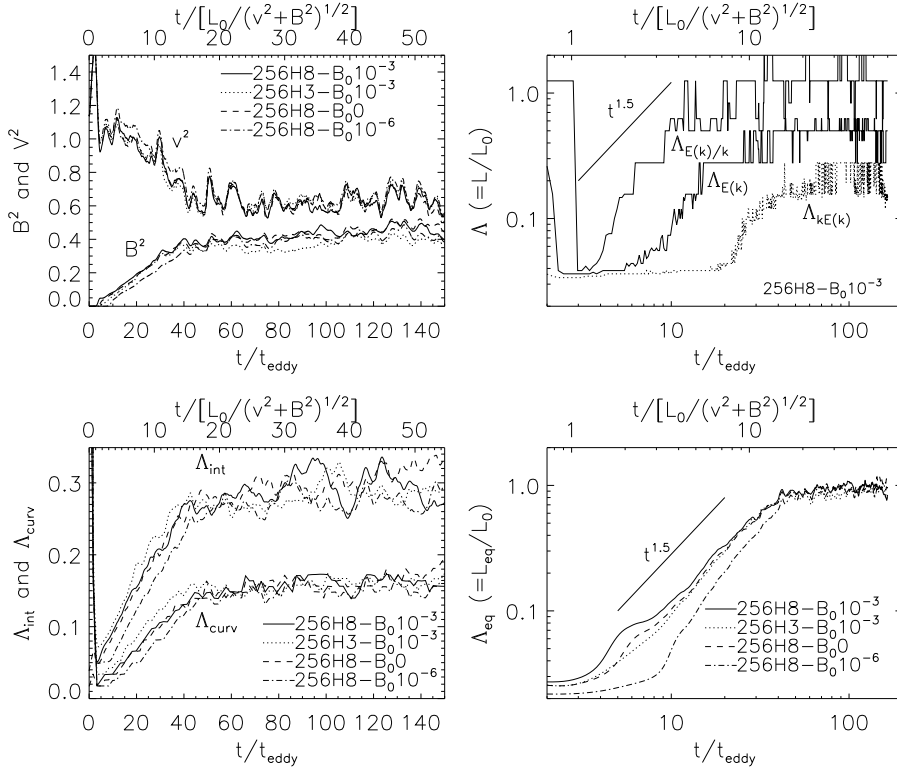


**Fig. 9** Top-left panel: The time evolution of  $V^2$  and  $B^2$  for four different runs. Here, the kinetic energy and magnetic energy densities are  $V^2/2$  and  $B^2/2$ , respectively. Top-right panel: Time evolution of peak scales of magnetic field spectrum,  $L_{E(k)}$ ,  $L_{kE(k)}$ , and  $L_{E(k)/k}$ . Bottom-right panel: Time evolution of the energy equipartition scale,  $L_{\text{eq}}$ . Bottom-left panel: Time evolution of the integral scale,  $L_{\text{int}}$ , and the curvature scale,  $L_{\text{curv}}$ .  $\Lambda$ 's are the scales normalized with the energy injection scale  $L_0$ . See the text for details.

The amplification of magnetic fields by turbulence dynamo is shown in the figure. It does not sensitively depend on the initial magnetic field strength once it is sufficiently weak as well as details of simulations including the dissipation prescription. The evolution of magnetic fields goes through three stages: the initially exponential growth when the back reaction of magnetic fields is negligible, then the linear growth when the back reaction starts to operate, and the final saturation. By fitting the evolution, we model the growth and saturation of magnetic field energy as

$$E_B = \begin{cases} 0.04 \times \exp [(t/t_{\text{eddy}} - 4)/0.36] & \text{for } t/t_{\text{eddy}} < 4 \\ (0.36/41) \times (t/t_{\text{eddy}} - 4) + 0.04 & \text{for } 4 < t/t_{\text{eddy}} < 45 \\ 0.4 & \text{for } t/t_{\text{eddy}} > 45 \end{cases} \quad (27)$$

Along with the amplification of magnetic field strength, the magnetic fields become coherent through the inverse cascade. For the quantification, different characteristic lengths of magnetic fields can be defined in MHD

turbulence: the peak scale of the spectrum of magnetic fields,  $L_{E(k)}$ , the scale containing the largest energy of magnetic fields,  $L_{kE(k)}$ , the peak scale of the spectrum of projected magnetic fields,  $L_{E(k)/k}$ , the energy equipartition scale,  $L_{\text{eq}} (= 2\pi/k_{\text{eq}})$ , defined as

$$\int_{k_{\text{eq}}}^{k_{\text{max}}} E_v(k) dk = \int_0^{k_{\text{max}}} E_b(k) dk, \quad (28)$$

the integral scale,  $L_{\text{int}}$ , defined as

$$L_{\text{int}} = 2\pi \frac{\int E_b(k)/k dk}{\int E_b(k) dk}, \quad (29)$$

and the curvature scale,  $L_{\text{curv}}$ , defined as a typical radius of curvature of field lines.

The rest of Figure 9 show the time evolution of characteristic lengths of magnetic fields. At saturation, the peak of magnetic field spectrum,  $L_{E(k)}$ , occurs at  $\sim L_0/2$ , where  $L_0$  is the energy injection scale, while the most energy containing scale,  $L_{kE(k)}$  is  $\sim L_0/5$ . During the stage of magnetic field amplification, the energy equipartition scale,  $L_{\text{eq}}$ , shows a power-law increase of  $\sim t^{1.5}$ , while the integral scale,  $L_{\text{int}}$ , and the curvature scale,  $L_{\text{curv}}$ , show a linear increase. The equipartition, integral, and curvature scales saturate at  $\sim L_0$ ,  $\sim 0.3L_0$ , and  $\sim 0.15L_0$ , respectively. See Cho and Ryu (2009) for further details of characteristic lengths in MHD turbulence with very weak or zero mean magnetic fields.

The results of the incompressible MHD turbulence simulation were convoluted to the data of the stimulation for the formation of the LSS of the universe to get the IGMF. For the estimation of the magnetic field strength, it was assumed that a fraction of the turbulence energy is converted into the magnetic energy. The fraction was expressed as a function of the number of local eddy turns over the age of the universe, so

$$\varepsilon_B = \varepsilon_{\text{curl}} \cdot \phi(\omega \times t_{\text{age}}). \quad (30)$$

For the fraction  $\phi(\omega \times t_{\text{age}})$ , the fitting formula in Equation (27) was used. Then, the magnetic field strength was calculated as  $(8\pi\varepsilon_B)^{1/2}$ .

The resulting magnetic field strength as a function of gas density and temperature is shown in the right panel of Figure 6. On average, the IGMF is predicted to be stronger in hotter and denser regions. It is because with the turbulence energy is larger in hotter and denser regions. Also the conversion factor,  $\phi$ , is larger in hotter and denser regions.

In the right panel of Figure 7, the volume-averaged and rms values of the magnetic field strength at a few redshifts for the gas in the hot IGM and WHIM are shown. Our scenario predicts that the magnetic field strength would be  $\langle B \rangle \gtrsim 1 \mu\text{G}$  inside clusters/groups,  $\sim 0.1 \mu\text{G}$  around clusters/groups, and  $\sim 10 \text{ nG}$  in filaments at the present universe. The magnetic fields should be much weaker in sheetlike structures and voids. But as noted in Section 5.1, turbulence is not fully developed there. So our estimation of the IGMF in those regions should not be applicable.

In each temperature range, the magnetic fields were stronger in the past at  $z \sim a$  few. Our calculation indicates that the vorticity has not changed much since  $z \sim a$  few (see the left panel of Figure 7), nor the vortical component of flow velocity (Ryu and Kang 2008). So the stronger magnetic fields in the past should be due to the higher density. We point that clusters were virialized around  $z \sim 1$  or so, so the density within the virial radius of  $\sim 1$  Mpc has not changed much since then. But our estimation of the magnetic field strength for the hot IGM with  $T > 10^7$  K also includes the gas in cluster outskirts, which extends far beyond the virial radius, up to several Mpc or even larger (see, e.g. Ryu et al. 2003); the density of the gas there was higher in the past. We also note that the magnetic fields, when averaged all over the computational box, were weaker in the past, because the fraction of the strong field regions was smaller.

Based on a kinetic theory, assuming the Kolmogorov spectrum for turbulence flow motions, Kulsrud et al. (1997) and Kulsrud and Zweibel (2008) estimated that the magnetic field strength in clusters would be a few  $\mu\text{G}$ . Our result agrees with the previous work. It also matches well with the observed strength of magnetic fields in the ICM, which is discussed in Section 1. On the other hand, our prediction of  $B \sim 10$  nG in filaments is within but lower than the upper limit of  $\sim 0.1\mu\text{G}$  which is imposed from RMs outside of clusters (Ryu et al. 1998, Xu et al. 2006).

The characteristic lengths of the IGMF in our scenario can be conjectured. In clusters, turbulence is near the saturation stage with  $t/t_{\text{eddy}} \sim 30$  (see Figures 7 and 9). Then, for instance, we may estimate that the peak scale of magnetic field spectrum and the integral scale would  $L_{E(k)}/L_0 \sim 0.4$  and  $L_{\text{int}}/L_0 \sim 0.2$ . If we take the energy injection scale  $L_0 \sim 100$  kpc, which is approximately the scale height of cluster core,  $L_{E(k)} \sim 40$  kpc and  $L_{\text{int}} \sim 20$  kpc, respectively. In filaments, on the other hand, with  $t/t_{\text{eddy}} \sim 10$ , turbulence is expected to be still in the linear growth stage, and  $L_{E(k)}/L_0 \sim 1/10$  and  $L_{\text{int}}/L_0 \sim 1/15$ . We may take the energy injection scale  $L_0 \sim 5$  Mpc, which is the typical thickness of filaments. Then,  $L_{E(k)} \sim 0.5$  Mpc and  $L_{\text{int}} \sim 0.3$  Mpc, respectively.

### 5.3 Contribution from AGNs

There is a possibility that the IGMF is further strengthened by the magnetic fields ejected through jets from black holes in AGNs (see, e.g., Kronberg et al. 2001). Strong magnetic fields almost certainly arise in accretion disks surrounding black holes. These fields may find their way into the IGM via magnetically dominated jets. The potential field strength due to this process can be estimated as follows (see, e.g., Hoyle 1969). The rotational energy associated with the central compact objects of mass  $M$  which power AGNs can be parametrized as  $fMc^2$  where  $f < 1$ . If we assume equipartition between rotational and magnetic energies within a central volume  $V_c$ , we find

$$B_c \sim \left( \frac{8\pi f M c^2}{V_c} \right)^{1/2}. \quad (31)$$



If this field then expands adiabatically to fill a volume  $V$  in the IGM, one finds  $B \sim B_c (V_c/V)^{2/3}$ . Considering the values of  $M = 10^9 M_\odot$ ,  $f = 0.1$ , and  $V \simeq (1 \text{ Mpc})^3$ , we get  $B \sim 10 \text{ nG}$ . Note this field strength is comparable to that estimated in filaments with turbulence dynamo. So this process may enhance the strength of the IGMF by a factor of two or so.

Although there are some RM observations that indicate strong magnetic fields in some of jets, however, it is not yet clear whether all jets are magnetically dominated. Also the details of the population of AGN jets and the volume filling fraction of magnetic fields in the universe by this process need to be further worked out.

## 6 Astrophysical Implications of the IGMF

The existence of the IGMF, especially in filaments, can have noticeable implications on a variety of astrophysical phenomena. In this section, we discuss two: the effect on the propagation of ultra-high energy cosmic rays (UHECRs) and the inducement of Faraday rotation.

### 6.1 Propagation of ultra-high energy cosmic rays

UHECRs are known to originate from extragalactic sources. Hence, on their path through the intergalactic space, the trajectories of UHECRs are deflected by the magnetic fields between sources and us, the IGMF as well as the galactic magnetic field (GMF). Das et al. (2008) studied the effect of the IGMF described in Section 5 on the propagation of UHECRs. Under the premise that the sources of UHECRs are strongly associated with the LSS of the universe, super-GZK protons of  $E \geq 10^{19} \text{ eV}$  were injected by AGN-like sources located inside clusters of galaxies. Then, the trajectories of the protons were followed, while taking account of the energy loss due to interactions with the cosmic microwave background (CMB) radiation. Das et al. (2008) found that the deflection of UHECR trajectories is caused mostly by the IGMF in filaments, rather than the the intracluster magnetic field in clusters; it is because filaments fill a larger fraction of volume, although their magnetic fields are weaker, than clusters. With the gyroradius of protons

$$r_g = 1 \text{ Mpc} \left( \frac{E_{\text{UHECR}}}{10^{19} \text{ eV}} \right) \left( \frac{B}{10 \text{ nG}} \right)^{-1}, \quad (32)$$

that is, with the gyroradius corresponding typical filament size for the magnetic fields typical in filaments, the deflection due to the IGMF in filaments is expected to be significant. Indeed, the deflection angle between the arrival direction of super-GZK protons and the sky position of their actual sources was found to be quite large with the mean value of  $\langle \theta \rangle \sim 15^\circ$  and the median value of  $\tilde{\theta} \sim 7 - 10^\circ$ .

The above deflection is much larger than the deflection by the GMF; the deflection angle due to the GMF was predicted to be a few degree (see, e.g., Takami and Sato 2008). As a matter of fact, the deflection angle of

$\langle\theta\rangle \sim 15^\circ$  is also much than the angular window of  $3.1^\circ$  used by the Auger collaboration in the study of the correlation between their highest energy UHECR events and nearby AGNs (The Pierre Auger Collaboration 2007). Although the deflection angle is large, Ryu et al. (2010) noticed that in the work of Das et al. (2008), the separation angle between the arrival direction of super-GZK protons and the sky position of nearest AGNs is substantially smaller with  $\langle S \rangle \sim 3.5 - 4^\circ$ , which is similar to the mean angular distance in the sky to nearest neighbors among AGNs. This mean separation angle is comparable to the angle used in the correlation study by the Auger collaboration. This is a direct consequence of the fact that the sources and us, as well as the IGMF, all trace the matter distribution of the universe. That is, although the IGMF described in Section 5 predicts larger deflection of UHECRs, it is not necessarily inconsistent with the intervening magnetic fields implied in the Auger experiment.

## 6.2 Faraday rotation induced by the IGMF

The IGMF described in Section 5 induces RM. With characteristic lengths smaller than the dimension of clusters or filaments, the inducement of RM is a random walk process; the standard deviation of RM is

$$\sigma_{\text{RM}} = 0.81 \bar{n}_e B_{\parallel\text{rms}} \sqrt{\left(\frac{3L_{\text{int}}}{4}\right)} L \text{ rad m}^{-2}, \quad (33)$$

where  $n_e$ ,  $B_{\parallel\text{rms}}$ , and  $L$  are in units of  $\text{cm}^{-3}$ ,  $\mu\text{G}$ , and pc, respectively (Cho and Ryu 2009).  $B_{\parallel\text{rms}}$  is the rms strength of line-of-sight magnetic field and  $L$  is the path length. Here, the coherence length for RM is given as  $l = (3/4)L_{\text{int}}$ . For clusters, with  $\bar{n}_e \sim 10^{-3} \text{ cm}^{-3}$ ,  $B_{\text{rms}} \sim$  a few  $\mu\text{G}$ ,  $L \sim 1 \text{ Mpc}$ , and  $L_{\text{int}} \sim 20 \text{ kpc}$  (see Section 5), we get  $\sigma_{\text{RM}} \sim 100 \text{ rad m}^{-2}$ , which agrees with the observed RM in clusters (Clarke et al. 2001). The magnetic field strength in filaments quoted in Section 5 is  $\langle B \rangle \sim 10 \text{ nG}$ . But the value depends on how it is averaged; that is,  $\langle B^2 \rangle^{1/2} \sim$  a few  $\times 10 \text{ nG}$ ,  $\langle \rho B \rangle / \langle \rho \rangle \sim 0.1 \mu\text{G}$ , and  $\langle (\rho B)^2 \rangle^{1/2} / \langle \rho^2 \rangle^{1/2} \sim$  a few  $\times 0.1 \mu\text{G}$ , in the warm-hot intergalactic medium (WHIM) with  $T = 10^5 - 10^7 \text{ K}$  which mostly composes filaments. The average value of  $\langle (\rho B)^2 \rangle^{1/2} / \langle \rho^2 \rangle^{1/2}$  should be relevant to RM. With  $\bar{n}_e \sim 10^{-5} \text{ cm}^{-3}$ ,  $B_{\text{rms}} \sim 0.3 \mu\text{G}$ ,  $L \sim 5 \text{ Mpc}$ , and  $L_{\text{int}} \sim 300 \text{ kpc}$ , we get  $\sigma_{\text{RM}} \sim 1 \text{ rad m}^{-2}$  through filaments.

Akahori and Ryu (2010) studied in details the RM due to the magnetic fields in filaments using the IGMF described in Section 5. Figure 10 shows a typical RM map in  $(28 h^{-1}\text{Mpc})^2$  area; the spatial distribution of RM traces the large-scale distribution of matter, showing two clusters and a filamentary structure containing several groups. The resultant RM is dominantly contributed by the density peak along line of sight. The rms of RM through filaments at the present universe was predicted to be  $\sim 1 \text{ rad m}^{-2}$ , which agrees with the estimation above (Cho and Ryu 2009). Figure 11 shows the two-dimensional power spectrum of the RM in the local universe within  $100 h^{-1} \text{ Mpc}$ ;  $P_{\text{RM}}(k) \sim |\text{RM}(\mathbf{k})|^2 k$ , where  $\text{RM}(\mathbf{k})$  is the Fourier transform

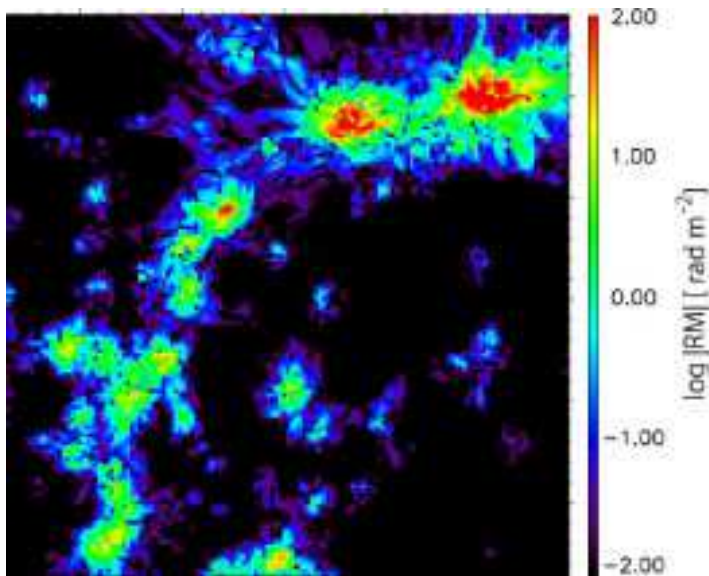


**Fig. 10** RM map of path length of  $L = 100 h^{-1}$  in the local universe o  $(28 h^{-1}\text{Mpc})^2$  area at  $z = 0$ .

of  $\text{RM}(\mathbf{x})$ . The power spectrum of RM peaks at  $k \sim 100$ , which corresponds to  $\sim 1 h^{-1}$  Mpc. In addition, Akahori and Ryu (2010) predicted that the probability distribution function (PDF) of  $|\text{RM}|$  through filaments follows the log-normal distribution. We note that  $\text{RM} \sim 1 \text{ rad m}^{-2}$  is an order of magnitude smaller than the values of  $|\text{RM}|$  toward the Hercules and Perseus-Pisces superclusters reported in Xu et al. (2006). The difference is mostly due to the mass-weighted path length; the value quoted by Xu et al. (2006) is about two orders of magnitude larger than ours.

$\text{RM} \sim 1 \text{ rad m}^{-2}$  due to the IGMF in filaments is too small to be confidently observed with currently available facilities. In addition, the galactic foreground of  $\sim 10 \text{ rad m}^{-2}$  (toward halo) poses an additional challenge for its observation. The next generation radio interferometers, however, are expected to be able to observe the RM. Particularly, the SKA could measure RM for  $\sim 10^8$  polarized extragalactic sources across the sky with an average spacing of  $\sim 60$  arcsec between lines of sight (papers in Carilli and Rawlings 2004) (Krause et al. 2009), enabling us to investigate the IGMF in the LSS of the universe.

## 7 Structure Formation and Magnetic Fields

The existence of magnetic fields in the early universe, although probably weak, can have consequences on the structure formation itself. In this section, we briefly review recent developments in our understanding of magnetized structure formation.

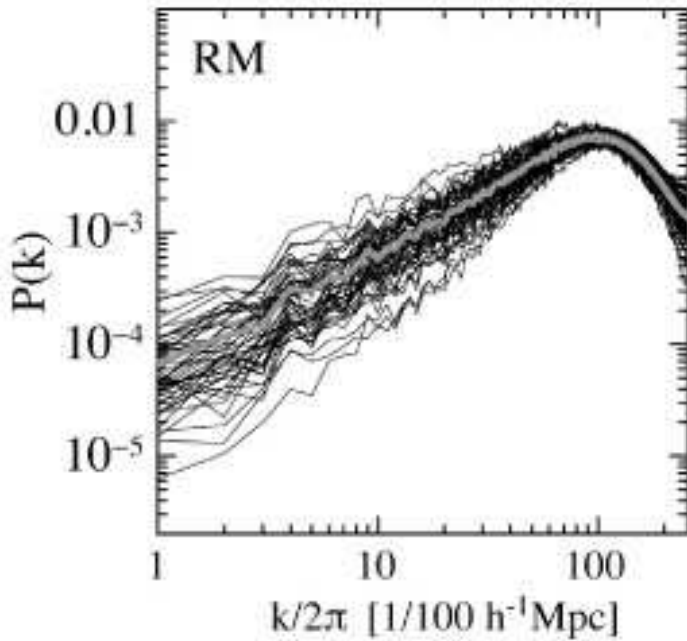


**Fig. 11** Two-dimensional power spectra of RM for  $3 \times 16$  two-dimensional projected maps from 16 simulations with different realizations of initial condition to compensate cosmic variance. The thick gray line shows the average.

### 7.1 The linear regime

Studies of magnetized structure formation go back to the late 1960s with the early efforts based on Newtonian gravity and the relativistic approaches being a relatively recent addition. All treatments typically work within the ideal MHD approximation and look at the effects of the magnetic Lorentz force on density inhomogeneities (Ruzmaikina and Ruzmaikin 1971, Wasserman 1978, Fennelly and Evans 1980, Kim et al. 1996, Battaner et al. 1997, Tsagas and Barrow 1997, Tsagas and Maartens 2000a). These effects generally come in the form of scalar, vector and (trace-free) tensor distortions. The former are those commonly referred to as density perturbations and represent over-densities or under-densities in the matter distribution. Vector inhomogeneities describe rotational (i.e. vortex-like) density perturbations. Finally, tensor-type density inhomogeneities correspond to shape distortions.<sup>1</sup> Following (Tsagas and Barrow 1997, Barrow et al. 2007), we define the scalar

$$\Delta \equiv \frac{a^2}{\rho} D^2 \rho, \quad (34)$$

<sup>1</sup> It should be made clear that trace-free tensor inhomogeneities (i.e. shape deformations) and pure-tensor distortions (i.e. gravitational waves) are two different types of perturbations.

which describes linear density perturbations and corresponds to the more familiar density contrast  $\delta\rho/\rho$ . Note that positive values for  $\Delta$  indicate over-densities and negative ones under-densities. Also,  $a$  is the cosmological scale factor and  $D^2 = D^a D_a$  is the 3-D Laplacian operator that corresponds to an observer moving with 4-velocity  $u_a$ .<sup>2</sup> In a perturbed, weakly magnetized and spatially flat Friedmann-Robertson-Walker (FRW) universe, the above defined scalar evolves according to

$$\dot{\Delta} = 3wH\Delta - (1+w)\mathcal{Z} + \frac{3}{2}c_a^2(1+w)H\mathcal{B}, \quad (35)$$

where over-dots denote proper-time derivatives (relative to the  $u_a$ -frame). Also,  $w = p/\rho$  is the (constant) barotropic index of the matter,  $H = \dot{a}/a$  is the background Hubble parameter (with  $\Theta = 3H$  there) and  $c_a^2 = B^2/\rho(1+w)$  is the square of the Alfvén speed. The variables  $\mathcal{Z} = a^2 D^2 \Theta$  and  $\mathcal{B} = (a^2/B^2)D^2 B^2$  describe linear inhomogeneities in the smooth Hubble expansion and in the magnetic energy density respectively. Then, to first order,

$$\dot{\mathcal{Z}} = -2H\mathcal{Z} - \frac{1}{2}\rho\dot{\Delta} + \frac{1}{4}c_a^2(1+w)\rho\dot{\mathcal{B}} - \frac{c_s^2}{1+w}D^2\Delta - \frac{1}{2}c_a^2D^2\mathcal{B} \quad (36)$$

and

$$\dot{\mathcal{B}} = \frac{4}{3(1+w)}\dot{\Delta}, \quad (37)$$

respectively. Note that  $c_s^2 = \dot{p}/\dot{\rho}$  is the square of the adiabatic sound speed and we have assumed that  $B^2 \ll \rho$ , given the relative weakness of the magnetic fields.

Equation (35) shows that magnetic fields are generic sources of linear density perturbations. Indeed, even if  $\Delta$  and  $\mathcal{Z}$  are zero initially,  $\dot{\Delta}$  will take nonzero values solely due to the magnetic presence. Also, Equation (37) ensures that perturbations in the magnetic field energy density evolve in tune with their matter counterparts (i.e.  $\mathcal{B} \propto \Delta$ ). Finally, we should emphasize that only the pressure part of the Lorentz force contributes to the linear relations (35) and (36).<sup>3</sup>

The system of Equations (35) – (37) has analytical solutions in the radiation and dust eras (Tsagas and Barrow 1997). Before equipartition, when  $w = 1/3 = c_s^2$ ,  $H = 1/2t$ ,  $\rho = 3/4t^2$  and  $c_a^2 = 3B^2/4\rho = \text{constant}$ , large-scale magnetized density perturbations obey a power-law solution. In particular,

<sup>2</sup> For an observer with 4-velocity  $u_a$  (so that  $u_a u^a = -1$ ), the tensor  $h_{ab} = g_{ab} + u_a u_b$  projects orthogonal to  $u_a$  and  $D_a = h_a^b \nabla_b$  defines the covariant derivative operator of the spatial hypersurfaces ( $g_{ab}$  is the space-time metric and  $\nabla_a$  the associated covariant derivative).

<sup>3</sup> The Lorentz force splits as  $\varepsilon_{abc} B^b \text{curl} B^c = D_a/2B^2 - B^b D_b B_a$ , with the former term corresponding to the magnetic pressure and the latter to the field's tension. The effects of the  $B$ -field on (scalar) density perturbations propagate via the divergence of the Lorentz force. To leading order, the latter is given by  $D^a(\varepsilon_{abc} B^b \text{curl} B^c) = D^2 B^2/2 - B^b D_b D^a B_a - KB^2/a^2$ , where  $K = 0, \pm 1$  represents the background 3-curvature index. Given that  $D^a B_a = 0$  at the ideal-MHD limit, the magnetic tension effects are not included in this perturbative level, unless the spatial curvature of the FRW model is accounted for (Tsagas and Maartens 2000a,b).

on super-horizon scales and keeping only the dominant growing and decaying modes, one arrives at (Tsagas and Maartens 2000a, Barrow et al. 2007)

$$\Delta = \mathcal{C}_1 t^{-1/2+10c_a^2/9} + \mathcal{C}_2 t^{1-4c_a^2/9}. \quad (38)$$

In the absence of magnetic fields, we recover the standard growing and decaying modes of  $\Delta \propto t$  and  $\Delta \propto t^{-1/2}$  respectively. So, the magnetic presence has reduced the growth rate of the density contrast by  $4c_a^2/9$ .

Well inside the horizon we can no longer ignore the role of the pressure gradients. There, the  $k$ -mode oscillates like a magneto-sonic wave with

$$\Delta_{(k)} \propto \sin \left[ c_s \left( 1 + \frac{2}{3} c_a^2 \right) \left( \frac{\lambda_H}{\lambda_k} \right)_0 \sqrt{\frac{t}{t_0}} \right], \quad (39)$$

where  $\lambda_k = a/k$  is the perturbed scale and  $\lambda_H = 1/H$  the Hubble horizon (Tsagas and Maartens 2000a, Barrow et al. 2007). Here, the magnetic pressure increases the effective sound speed and therefore the oscillation frequency. The former makes the Jeans length larger than in non-magnetized models. The latter brings the peaks of short-wavelength oscillations in the radiation density closer, leaving a potentially observable signature in the CMB spectrum (Adams et al. 1996).

When dust dominates,  $w = 0 = c_s^2$ ,  $H = 2/3t$ ,  $\rho = 4/3t^2$  and  $c_a^2 = B^2/\rho \propto t^{-2/3}$ . Then, on superhorizon scales, the main growing and decaying modes of the density contrast are (Tsagas and Barrow 1997, Barrow et al. 2007)

$$\Delta = \mathcal{C}_1 t^{\alpha_1} + \mathcal{C}_2 t^{\alpha_2}, \quad (40)$$

with  $\alpha_{1,2} = -[1 \pm 5\sqrt{1 - (32/75)(c_a \lambda_H/\lambda_k)_0^2}]/6$ . In the absence of magnetic fields we recover again the standard solution with  $\alpha_1 = 2/3$  and  $\alpha_2 = -1$ . Thus, as with the radiation era before, the magnetic presence slows down the growth rate of density perturbations. Also, since  $\mathcal{B} \propto \Delta$  [see Equation (37)], the above describes the linear evolution of the magnetic energy-density perturbations as well. This means that cosmological magnetic fields trapped inside an overdense region of the post-recombination universe could grow by approximately two to three orders of magnitude. Note that the aforementioned increase is different from the one occurring during the subsequent, nonlinear contraction of a protogalactic cloud (see Section 7.2 below).

The field pressure also leads to a magnetically induced Jeans length, below which density perturbations cannot grow (Subramanian and Barrow 1998, Sethi and Subramanian 2005). As a fraction of the Hubble radius, this purely magnetic Jeans scale is (Tsagas and Maartens 2000a, Barrow et al. 2007)

$$\lambda_J \sim c_a \lambda_H. \quad (41)$$

Setting  $B \sim 10^{-9}$  G, which is the maximum homogeneous field strength allowed by the CMB (Zeldovich 1970a, Barrow et al. 1997), we find that  $\lambda_J \sim 10$  kpc. Alternative, magnetic fields close to  $10^{-7}$  G, like those found in galaxies and galaxy clusters, give  $\lambda_J \sim 1$  Mpc. The latter lies intriguingly close to the size of a cluster of galaxies.

Overall, the magnetic effect on density perturbations is rather negative. Although magnetic fields generate this type of distortions, they do not help them to grow. Instead, the magnetic presence either suppresses the growth rate of density perturbations, or increases the effective Jeans length and therefore the domain where these inhomogeneities cannot grow. This negative role of magnetic fields, which was also observed in the Newtonian treatment of (Ruzmaikina and Ruzmaikin 1971), reflects the fact that only the pressure part of the Lorentz force has been incorporated into the equations. When the tension component (i.e. the elasticity of the field lines) is also accounted for, the overall magnetic effect can change and in some cases it could even reverse (Tsagas and Maartens 2000b).

Magnetic fields also induce and affect rotational, vortex-like, density inhomogeneities (Wasserman 1978, Tsagas and Maartens 2000a). To linear order, these are described by the vector  $\mathcal{W}_a = -(a^2/2\rho)\varepsilon_{abc}D^bD^c\rho$ , with  $\varepsilon_{abc}$  representing the 3-D Levi-Civita tensor. Then, on a spatially flat FRW background,

$$\ddot{\mathcal{W}}_a = -4H\dot{\mathcal{W}}_a - \frac{1}{2}\rho\mathcal{W}_a + \frac{1}{3}c_a^2D^2\mathcal{W}_a, \quad (42)$$

after matter-radiation equality (Tsagas and Maartens 2000a, Barrow et al. 2007). Defining  $\lambda_a = c_a\lambda_H$  as the Alfvén horizon, we may write the associated solution in the form

$$\mathcal{W}_{(k)} = \mathcal{C}_1t^{\alpha_1} + \mathcal{C}_2t^{\alpha_2}, \quad (43)$$

with  $\alpha_{1,2} = -[5 \pm \sqrt{1 - (48/9)(\lambda_a/\lambda_k)_0^2}]/6$ . On scales far exceeding the Alfvén horizon,  $\lambda_a \ll \lambda_k$  and the perturbed mode decays as  $\mathcal{W} \propto t^{-2/3}$ . This rate is considerably slower than  $\mathcal{W} \propto t^{-1}$ , the decay rate associated with magnetic-free dust cosmologies. Well inside  $\lambda_a$ , on the other hand, magnetized vortices oscillate like Alfvén waves, with (Tsagas and Maartens 2000a)

$$\mathcal{W}_{(k)} \propto t^{-5/6} \cos \left[ \frac{2\sqrt{3}}{9} \left( \frac{\lambda_a}{\lambda_k} \right)_0 \ln t \right]. \quad (44)$$

Thus, the effect of magnetic fields on a given vortex mode is to reduce its standard depletion rate. Analogous is the magnetic effect on  $\omega_a$ , namely on the vorticity proper. Hence, magnetized cosmologies appear to rotate faster than their magnetic-free counterparts. In contrast to density perturbations, magnetic fields seem to favor the presence of vorticity. This qualitative difference should probably be attributed to the fact that the tension part of the Lorentz force also contributes to Equation (42).

In addition to scalar and vector perturbations, magnetic fields also generate and affect tensor-type inhomogeneities that describe shape-distortions in the density distribution (Tsagas and Maartens 2000a). An initially spherically symmetric inhomogeneity, for example, will change shape due to the magnetically induced anisotropy. All these effects result from the Lorentz force. Even when the latter is removed from the system, however, magnetic fields remain active. Due to its energy density and anisotropic nature, for example, magnetism affects both the local and long-range gravitational fields. The anisotropic magnetic pressure, in particular, leads to shear distortions and subsequently to gravitational-wave production (Caprini and Durrer

2002, Tsagas 2002, Wang 2010). Overall, magnetic fields are a very versatile source. They are also rather unique in nature, since they are the only known vector source of energy. An additional unique magnetic feature, which remains relatively unexplored, is the field's tension. When we add to all these the widespread presence of magnetic fields in the universe, it is not unreasonable to say that no realistic structure formation scenario should a priori exclude them.

## 7.2 Aspects of the nonlinear regime

The evolution of large-scale magnetic fields during the nonlinear stages of structure formation is addressed primarily by means of numerical simulations. The reason is the high complexity of the nonlinear MHD equations, which considerably hampers analytical studies, unless certain simplifying assumptions are imposed.

The simplest approximation is to assume spherically symmetric compression. Realistic collapse, however, is not isotropic. In fact, when magnetic fields are present, their generically anisotropic nature makes the need to go beyond spherical symmetry greater. Certain aspects of anisotropic contraction can be analytically studied within the Zeldovich approximation (Zeldovich 1970b). The latter is based on a simple ansatz, which extrapolates to the nonlinear regime a well known linear result. The assumption is that the irrotational and acceleration-free linear motion of dust, also holds during the early nonlinear stages of galaxy formation. This allows the analytical treatment of the nonlinear equations, leading to solutions that describe anisotropic (one dimensional) collapse and to the formation of the well-known Zeldovich pancakes.

Suppose that magnetic fields are frozen into a highly conductive protogalactic cloud that is falling into the (Newtonian) potential wells formed by the Cold Dark Matter (CDM) sector.<sup>4</sup> Relative to the physical coordinate system  $\{r^\alpha\}$ , the motion of the fluid velocity is  $u_\alpha = 3Hr_\alpha + v_\alpha$ , where  $H = \dot{a}/a$  is the Hubble parameter of the unperturbed FRW background and  $v_\alpha$  is the peculiar velocity of the fluid (with  $\alpha = 1, 2, 3$ ). Then, the magnetic field induction equation reads (Bruni et al. 2003)

$$\dot{B}_\alpha = -2HB_\alpha - \frac{2}{3}\vartheta B_\alpha + \sigma_{\alpha\beta}B^\beta, \quad (45)$$

where  $\vartheta = \partial^\alpha v_\alpha$  and  $\sigma_{\alpha\beta} = \partial_{\langle\beta} v_{\alpha\rangle}$  are the peculiar volume scalar and the peculiar shear tensor respectively.<sup>5</sup> The former takes negative values (i.e.  $\vartheta < 0$ ), since we are dealing with a protogalactic cloud that has started to

<sup>4</sup> The Newtonian theory is a very good approximation, since we are dealing with non-relativistic matter and the scales of interest are well inside the curvature radius of the universe.

<sup>5</sup> When dealing with purely baryonic collapse, the Zeldovich ansatz only holds during the early stages of the nonlinear regime, when the effects of the fluid pressure are negligible. Assuming that the contraction is driven by non-baryonic CDM, means that we can (in principle) extend the domain of the Zeldovich approximation further.



turn around and collapse. Also note that the first term in the right-hand side of Equation (45) reflects the background expansion, the second is due to the peculiar contraction and the last carries the anisotropic effects. Introducing the rescaled magnetic field  $\mathcal{B}_\alpha = a^2 B_\alpha$ , the above expression recasts into

$$\mathcal{B}'_\alpha = -\frac{2}{3} \tilde{\vartheta} \mathcal{B}_\alpha + \tilde{\sigma}_{\alpha\beta} \mathcal{B}^\beta, \quad (46)$$

with primes indicating differentiation with respect to the scale factor. Also  $\vartheta = aH\tilde{\vartheta}$  and  $\sigma_{\alpha\beta} = aH\tilde{\sigma}_{\alpha\beta}$ , where  $\tilde{\vartheta} = \partial^\alpha \tilde{v}_\alpha$  and  $\tilde{\sigma}_{\alpha\beta} = \partial_{\langle\beta} \tilde{v}_{\alpha\rangle}$  (with  $\tilde{v}_\alpha = ax'_\alpha$  and  $v_\alpha = aH\tilde{v}_\alpha$ ). In the shear eigen-frame,  $\tilde{\sigma}_{\alpha\beta} = (\tilde{\sigma}_{11}, \tilde{\sigma}_{22}, \tilde{\sigma}_{33})$  and Equation (46) leads to

$$\mathcal{B}'_1 = -\frac{2}{3} \tilde{\vartheta} \mathcal{B}_1 + \tilde{\sigma}_{11} \mathcal{B}_1, \quad (47)$$

with exactly analogous relations for the rest of the magnetic components. The resulting system describes the second-order evolution of magnetic fields, which is frozen-in with the highly conductive matter of a collapsing protogalaxy, within the limits of the Zeldovich approximation. To obtain analytical solutions, we recall that in the absence of rotation and acceleration, the peculiar volume scalar is given by

$$\tilde{\vartheta} = \frac{\lambda_1}{1+a\lambda_1} + \frac{\lambda_2}{1+a\lambda_2} + \frac{\lambda_3}{1+a\lambda_3}, \quad (48)$$

At the same time,

$$\tilde{\sigma}_{11} = \frac{\lambda_1}{1+a\lambda_1} - \frac{1}{3} \tilde{\vartheta}, \quad (49)$$

while analogous expressions hold for the other two shear eigenvalues. Note that  $\lambda_1, \lambda_2$  and  $\lambda_3$  are the eigenvalues of the initial tidal field that determine the nature of the collapse (Matarrese 1996, Bruni 1996). One-dimensional collapse along, say, the third eigen-direction is characterized by  $\lambda_1 = 0 = \lambda_2$  and by  $\lambda_3 < 0$ . In that case, the pancake singularity is reached as  $a \rightarrow -1/\lambda_3$ . Spherically symmetric collapse, on the other hand, has  $\lambda_1 = \lambda_2 = \lambda_3 = \lambda < 0$ . Then, we have a point-like singularity when  $a \rightarrow -1/\lambda$ .

Substituting, Equations (48) and (49) into the right-hand side of Equation (47) we arrive at the solution

$$B_1 = B_1^0 \left[ \frac{(1+a_0\lambda_2)(1+a_0\lambda_3)}{(1+a\lambda_2)(1+a\lambda_3)} \right] \left( \frac{a_0}{a} \right)^2, \quad (50)$$

for the first of the magnetic components. A similar calculation leads to exactly analogous equations for  $B_2$  and  $B_3$ . The zero suffix in the above indicates a given time during the protogalactic collapse. The ratio  $a_0/a$  in parentheses reflects the magnetic dilution due to the background expansion and the brackets monitor the increase in the field's strength caused by the collapse of the protogalactic cloud. According to (50), when dealing with pancake collapse along the third eigen-direction, the  $B_3$ -component decays as  $a^{-2}$ ,

while the other two increase arbitrarily as  $a \rightarrow -1/\lambda_3$ . Alternatively, during a spherically symmetric contraction, the magnetic field evolve as

$$B = B_0 \left( \frac{1 + a_0 \lambda}{1 + a \lambda} \right)^2 \left( \frac{a_0}{a} \right)^2. \quad (51)$$

Here, all the magnetic components diverge as we approach the point singularity (i.e. for  $a \rightarrow -1/\lambda$ ). Comparing the two results, we deduce that the anisotropic (pancake) collapse leads to a stronger increase as long as  $\lambda_3 < \lambda$ . The later is always satisfied, provided that the initial conditions are the same for both types of collapse, given that  $\lambda_3 = \tilde{\vartheta}_0/(1 - a_0 \tilde{\vartheta}_0)$  and  $\lambda = \tilde{\vartheta}_0/(3 - a_0 \tilde{\vartheta}_0)$  [see expression (48) above].

Our qualitative analysis indicates that magnetic fields trapped in an anisotropically contracting protogalactic cloud will increase beyond the limits of the idealized spherically symmetric collapse. Also, the amplified magnetic fields will end up essentially confined to the galactic plane. Quantitatively, the achieved final strength depends on the time the magnetic back-reaction has grown strong enough to halt the collapse (Zeldovich et al. 1983). Thus, the longer the anisotropic collapse persists, the stronger the residual magnetic fields. The analytical study of (Bruni et al. 2003), in particular, showed that (realistically speaking) the anisotropy could add one or two orders of magnitude to the magnetic strength achieved through conventional isotropic compression. These results appear in very good agreement with numerical studies simulating shear and tidal effects on the magnetic field evolution in galaxies and galaxy clusters (Roettiger et al. 1999, Dolag et al. 2002).

## 8 Summary

The cosmic web, a network of filaments and nodes wherein most galaxies reside, is a prediction of the highly successful  $\Lambda$ CDM cosmology and appears to be borne out by by simulations and observations. The web is filled with an ionized plasma, the IGM, which is expected to be permeated by magnetic fields. In this chapter, we reviewed recent developments in our theoretical understanding of the nature and origin of IGMF with a special focus on fields outside of clusters. We addressed two basic questions: First, “Can the process of structure formation generate seed magnetic fields and amplify them?” and second, “What role do magnetic fields play in structure formation and in other astrophysical processes?” We presented several plasma physics mechanisms for the generation of seed magnetic fields, and showed that these fields could be amplified during the first star formation and later during the formation of the cosmic web. We saw that magnetic fields with a strength of  $\langle B \rangle \sim 10$  nG are expected in filaments at the present universe, while magnetic fields should be stronger in and around clusters/groups. We then discussed the effects and implications of magnetic fields on the formation of the first stars. We also presented a formal treatment of the evolution of density perturbations in the presence of magnetic fields and their effects on the formation of structures.

Magnetic fields in the IGM are difficult to be observed, mainly due to the weak nature of them, as well as due to the diffuseness of the media. However, the next generation radio interferometers including the Square Kilometer Array (SKA), and upcoming SKA pathfinders, the Australian SKA Pathfinder (ASKAP) and the South African Karoo Array Telescope (MeerKAT), as well as the Low Frequency Array (LOFAR) will enable us to investigate magnetic fields outside clusters with high-sensitivity observations of synchrotron radiation and RM (see, e.g., papers in Carilli and Rawlings 2004).

**Acknowledgements** The work of DR was supported by the National Research Foundation of Korea through grant 2007-0093860. The work of DS was supported by a funding from the European Community's Seventh Framework Programme (/FP7/2007-2013/) under grant agreement No 229517. The work of LMW was supported by a Discovery Grant from the Natural Sciences and Engineering Research Council of Canada.

## References

- T. Abel, G. L. Bryan, M. L. Norman, The formation of the first star in the universe. *Science* **295**, 93-98 (2002). doi:10.1126/science.1063991
- A. Achterberg, J. Wiersma, The Weibel instability in relativistic plasmas. I. Linear theory. *Astron. Astrophys.* **475**, 1-36 (2007). doi:10.1051/0004-6361/20065365
- J. Adams, U. H. Danielson, D. Grasso, H. R. Rubinstein, Distortion of the acoustic peaks in the CMBR due to a primordial magnetic field. *Phys. Lett. B* **388**, 253-258 (1996). doi:10.1016/S0370-2693(96)01171-9
- T. Akahori, D. Ryu, Faraday rotation measure due to the intergalactic magnetic field. *Astrophys. J.* **723**, 467-481 (2010). doi:10.1088/0004-637X/723/1/476
- J. Aleksić and MAGIC Collaboration, Search for an extended VHE  $\gamma$ -ray emission from Mrk 421 and Mrk 501 with the MAGIC Telescope. *Astron. Astrophys.* **524**, id. A77 (2010). doi:10.1051/0004-6361/201014747
- T. G. Arshakian, R. Beck, M. Krause, D. Sokoloff, Evolution of magnetic fields in galaxies and future observational tests with the Square Kilometre Array. *Astron. Astrophys.* **494**, 21-32 (2009). doi:10.1051/0004-6361:200810964
- J. D. Barrow, P. G. Ferreira, J. Silk, Constraints on a primordial magnetic field. *Phys. Rev. Lett.* **78**, 3610-3613 (1997). doi:10.1103/PhysRevLett.78.3610
- J. D. Barrow, R. Maartens, C. G. Tsagas, Cosmology with inhomogeneous magnetic fields. *Phys. Rep.* **449**, 131-171 (2007). doi:10.1016/j.physrep.2007.04.006
- E. Battaner, E. Florido, J. Jimenez-Vicente, Magnetic fields and large scale structure in a hot universe. I. General equations. *Astron. Astrophys.* **326**, 13-22 (1997).
- A. R. Bell, Turbulent amplification of magnetic field and diffusive shock acceleration of cosmic rays. *Mon. Not. Royal Astron. Soc.* **353**, 550-558 (2004). doi:10.1111/j.1365-2966.2004.08097.x
- L. Biermann, Über den Ursprung der Magnetfelder auf Sternen und im interstellaren Raum. *Z. Naturforsch. A* **5**, 65-71 (1950).
- A. Bonafede, L. Feretti, M. Murgia, F. Govoni, G. Giovannini, G., D. Dallacasa, K. Dolag, G. B. Taylor, The Coma cluster magnetic field from Faraday rotation measures. *Astron. Astrophys.* **513**, A30 (2010). doi:10.1051/0004-6361/200913696
- J. R. Bond, L. Kofman, D. Pogosyan, How filaments of galaxies are woven into the cosmic web. *Nature* **380**, 603-606 (1996). doi:10.1038/380603a0
- A. Brandenburg, K. Subramanian, Astrophysical magnetic fields and nonlinear dynamo theory. *Phys. Rep.* **417**, 1-209 (2005). doi:10.1016/j.physrep.2005.06.005
- A. Brandenburg, K. Subramanian, D. D. Sokoloff Turbulent dynamos. in this volume (2010).

- 
- V. Bromm, A. Loeb, Formation of the first supermassive black holes. *Astrophys. J.* **596**, 34-46 (2003). doi:10.1086/377529
- S. Brown, D. Farnsworth, L. Rudnick, Cross-correlation of diffuse synchrotron and large-scale structures. *Mon. Not. Royal Astron. Soc.* **402**, 2-6 (2010). doi:10.1111/j.1365-2966.2009.15867.x
- M. Brüggen, A. Bykov, D. Ryu, H. Röttgering, Magnetic fields, relativistic particles, and shock waves in cluster outskirts in this volume (2010).
- M. Bruni, Cosmological collapses of irrotational dust. in *Mapping, measuring and modelling the universe*, Ed. P. Coles, V. Martinez, M.-J. Pons-Borderia, ASP Conference Series **94**, 31-36 (1996).
- M. Bruni, R. Maartens, C. G. Tsagas, Magnetic field amplification in cold dark matter anisotropic collapse. *Mon. Not. Royal Astron. Soc.* **338**, 785-789 (2003). doi:10.1046/j.1365-8711.2003.06095.x
- C. Caprini, R. Durrer, Gravitational wave production: A strong constraint on primordial magnetic fields. *Phys. Rev. D* **65**, 023517 (2002). doi:10.1103/PhysRevD.65.023517
- C. L. Carilli, S. Rawlings, *Science with the Square Kilometre Array* (New A Rev. **48**, 2004).
- C. L. Carilli, G. B. Taylor, Cluster magnetic fields. *Ann. Rev. Astron. Astrophys.* **40**, 319-348 (2002). doi:10.1146/annurev.astro.40.060401.093852
- R. Cassano, G. Brunetti, T. Venturi, G. Setti, D. Dallacasa, S. Giacintucci, S. Bardelli, Revised statistics of radio halos and the reacceleration model. *Astron. Astrophys.* **480**, 687-697 (2008). doi:10.1051/0004-6361:20078986
- R. A. Cassidy, M. T. Elford, The mobility of  $\text{Li}^+$  ions in helium and argon. *Aust. J. Phys.* **38**, 587-601 (1985).
- R. Cen, J. P. Ostriker, Where are the baryons? *Astrophys. J.* **514**, 1-6 (1999). doi:10.1086/306949
- R. Cen, J. P. Ostriker, Where are the baryons? II. Feedback effects. *Astrophys. J.* **650**, 560-572 (2006). doi:10.1086/506505
- R. Cen, J. P. Ostriker, J. X. Prochaska, A. M. Wolfe, Metallicity evolution of damped Ly systems in  $\Lambda$ CDM cosmology. *Astrophys. J.* **598**, 741-755 (2003). doi:10.1086/378881
- J. Cho, D. Ryu, Characteristic lengths of magnetic field in magnetohydrodynamic turbulence. *Astrophys. J.* **705**, L90-L94 (2009). doi:10.1088/0004-637X/705/1/L90
- J. Cho, E. T. Vishniac, The generation of magnetic fields through driven turbulence. *Astrophys. J.* **538**, 217-225 (2000). doi:10.1086/309127
- J. Cho, E. T. Vishniac, A. Beresnyak, A. Lazarian, D. Ryu, Growth of magnetic fields induced by turbulent motions. *Astrophys. J.* **693**, 1449-1461 (2009). doi:10.1088/0004-637X/693/2/1449
- P. C. Clark, S. C. O. Glover, R. S. Klessen, V. Bromm, Gravitational fragmentation in turbulent primordial gas and the initial mass function of Population III stars. *Astrophys. J.* **727**, id. 110 (2011). doi:10.1088/0004-637X/727/2/110
- T. E. Clarke, Faraday rotation observations of magnetic fields in galaxy clusters. *J. Korean Astron. Soc.* **37**, 337-342 (2004).
- T. E. Clarke, P. P. Kronberg, H. Böhringer, A new radio-X-ray probe of galaxy cluster magnetic fields. *Astrophys. J.* **547**, L111-L114 (2001). doi:10.1086/318896
- S. Das, H. Kang, D. Ryu, J. Cho, Propagation of ultra-high-energy protons through the magnetized cosmic web. *Astrophys. J.* **682**, 29-38 (2008). doi:10.1086/588278
- G. Davies, L.M. Widrow, A possible mechanism for generating galactic magnetic fields. *Astrophys. J.* **540**, 755-764 (2000). doi:10.1086/309358
- C. D. Dermer, M. Cavadini, S. Razzaque, J. D. Finke, J. Chiang, B. Lott, Time delay of cascade radiation for TeV blazars and the measurement of the intergalactic magnetic field. *Astrophys. J. Lett.* **733**, L21-L24 (2011). doi:10.1088/2041-8205/733/2/L21
- A. S. Dickinson, M. S. Lee, W. A. Lester, Jr., Close-coupling calculation of  $\text{Li}^+ - \text{H}_2$  diffusion cross sections. *J. Phys. B* **15**, 1371-1376 (1982). doi:10.1088/0022-3700/15/9/013

- 
- K. Dolag, M. Bartelmann, H. Lesch, Evolution and structure of magnetic fields in simulated galaxy clusters. *Astron. Astrophys.* **387**, 383-395 (2002). doi:10.1051/0004-6361:20020241
- J. Donnert, K. Dolag, H. Lesch, E. Müller, Cluster magnetic fields from galactic outflows. *Mon. Not. Royal Astron. Soc.* **392**, 1008-1021 (2009). doi:10.1111/j.1365-2966.2008.14132.x
- A. J. Fennelly, C. R. Evans, Magnetohydrodynamic perturbations of Robertson-Walker universes and of anisotropic Bianchi type-I universes. *Nuovo Cim. B* **60**, 1-45 (1980). doi:10.1007/BF02723065
- C. Federrath, S. Sur, D. R. G. Schleicher, R. Banerjee, R. S. Klessen, A new jeans resolution criterion for (M)HD simulations of self-gravitating gas: Application to magnetic field amplification by gravity-driven turbulence. *Astrophys. J.* **71**, id. 62 (2011). doi:10.1088/0004-637X/731/1/62
- B. D. Fried, Mechanism for instability of transverse plasma waves. *Phys. Fluids* **2**, 337 (1959). doi:10.1063/1.1705933
- S. Fromang, S. A. Balbus, C. Terquem, J. De Villiers, Evolution of self-gravitating magnetized disks. II. Interaction between magnetohydrodynamic turbulence and gravitational instabilities. *Astrophys. J.* **616**, 364-375 (2004). doi:10.1086/424829
- S. C. O. Glover, D. W. Savin, Is  $H_+^3$  cooling ever important in primordial gas? *Mon. Not. Royal Astron. Soc.* **393**, 911-948 (2009). doi:10.1111/j.1365-2966.2008.14156.x
- F. Govoni, L. Feretti, Magnetic fields in clusters of galaxies. *Int. J. Mod. Phys. D* **13**, 1549-1594 (2004). doi:10.1142/S0218271804005080
- D. Grasso, H. R. Rubinstein, Magnetic fields in the early universe. *Phys. Rep.* **348**, 163-266 (2001). doi:10.1016/S0370-1573(00)00110-1
- A. Gruzinov, Gamma-ray burst phenomenology, shock dynamics, and the first magnetic fields. *Astrophys. J. Lett.* **563**, L15-L18 (2001). doi:10.1086/324223
- A. Gruzinov, E. Waxman, Gamma-ray burst afterglow: Polarization and analytic light curves. *Astrophys. J.* **511**, 852-861 (1999). doi:10.1086/306720
- D. Guidetti, M. Murgia, F. Govoni, P. Parma, L. Gregorini, H. R. deRuiter, R. A. Cameron, R. Fanti, The intracluster magnetic field power spectrum in Abell 2382. *Astron. Astrophys.* **483**, 699-713 (2008). doi:10.1051/0004-6361:20078576
- N. E. L. Haugen, A. Brandenburg, W. Dobler, Simulations of non-helical hydromagnetic turbulence. *Phys. Rev. e* **70**, 016308 (2004a). doi:10.1103/PhysRevE.70.016308
- N. E. L. Haugen, A. Brandenburg, W. Dobler, High-resolution simulations of nonhelical MHD turbulence. *Astrophys. Space Sci.* **292**, 53-60 (2004b). doi:10.1023/B:ASTR.0000045000.08395.a3
- N. E. L. Haugen, A. Brandenburg, A. J. Mee, Mach number dependence of the onset of dynamo action. *Mon. Not. Royal Astron. Soc.* **353**, 947-952 (2004c). doi:10.1111/j.1365-2966.2004.08127.x
- F. Hoyle, Magnetic fields and highly condensed objects. *Nature* **223**, 936 (1969). doi:10.1038/223936a0
- C. H. Jaroschek, M. Hoshino, Radiation dominated relativistic current sheets. *Phys. Rev. Lett.* **103**, 075002 (2009). doi:10.1103/PhysRevLett.103.075002
- C. H. Jaroschek, M. Hoshino, H. Lesch, R. A. Treumann, Stochastic particle acceleration by the forced interaction of relativistic current sheets. *Adv. Space Res.* **41**, 481-490 (2008). doi:10.1016/j.asr.2007.07.001
- C. H. Jaroschek, H. Lesch, R. A. Treumann, Ultra-relativistic plasma shell collisions in gamma-ray burst sources: Dimensional effects and the final steady state magnetic field. *Astrophys. J.* **618**, 822-831 (2005). doi:10.1086/426066
- H. Kang, D. Ryu, R. Cen, J. P. Ostriker, Cosmological shock waves in the large-scale structure of the universe: Nongravitational effects. *Astrophys. J.* **669**, 729-740 (2007). doi:10.1086/521717
- H. Kang, D. Ryu, R. Cen, D. Song, Shock-heated gas in the large-scale structure of the universe. *Astrophys. J.* **620**, 21-30 (2005). doi:10.1086/426931
- K. T. Kim, P. P. Kronberg, P. D. Dewdney, T. L. Landecker, The halo and magnetic field of the Coma cluster of galaxies. *Astrophys. J.* **355**, 29-37 (1990).

- doi:10.1086/168737
- K. T. Kim, P. P. Kronberg, G. Giovannini, T. Venturi, Discovery of intergalactic radio emission in the Coma-A1367 supercluster. *Nature* **341**, 720-723 (1989). doi:10.1038/341720a0
- E.-J. Kim, A. V. Olinto, R. Rosner, Generation of density perturbations by primordial magnetic fields. *Astrophys. J.* **468**, 28-50 (1996). doi:10.1086/177667
- E. W. Kolb, M. S. Turner, *The early universe* (Addison-Wesley, Redwood City, 1990).
- M. Krause, P. Alexander, R. Bolton, J. Geisbüsch, D. A. Green, J. Riley, Measurements of the cosmological evolution of magnetic fields with the Square Kilometre Array. *Mon. Not. Royal Astron. Soc.* **400**, 646-656 (2009). doi:10.1111/j.1365-2966.2009.15489.x
- P. P. Kronberg, Q. W. Dufton, H. Li, S. A. Colgate, Magnetic energy of the intergalactic medium from galactic black holes. *Astrophys. J.* **560**, 178-186 (2001). doi:10.1086/322767
- R. M. Kulsrud, R. Cen, J. P. Ostriker, D. Ryu, The protogalactic origin for cosmic magnetic fields. *Astrophys. J.* **480**, 481-491 (1997). doi:10.1086/303987
- R. M. Kulsrud, E. G. Zweibel, On the origin of cosmic magnetic fields. *Rep. Prog. Phys.* **71**, 046901 (2008). doi:10.1088/0034-4885/71/4/046901
- M. I. Large, D. S. Mathewson, C. G. T. Haslam, A high-resolution survey of the Coma cluster of galaxies at 408 Mc./s. *Nature* **183**, 1663-1664 (1959). doi:10.1038/1831663a0
- R. B. Larson, Numerical calculations of the dynamics of collapsing proto-star. *Mon. Not. Royal Astron. Soc.* **145**, 271-295 (1969).
- A. Lazarian, Diffusion-generated electromotive force and seed magnetic field problem. *Astron. Astrophys.* **264**, 326-330 (1992).
- M. N. Machida, S. Inutsuka, T. Matsumoto, T. High- and low-velocity magnetized outflows in the star formation process in a gravitationally collapsing cloud. *Astrophys. J.* **676**, 1088-1108 (2008). doi:10.1086/528364
- M. N. Machida, K. Omukai, T. Matsumoto, S. Inutsuka, The first jets in the universe: protostellar jets from the first stars. *Astrophys. J. Lett.* **647**, L1-L4 (2006). doi:10.1086/507326
- H. Maki, H. Susa, Dissipation of magnetic flux in primordial gas clouds. *Astrophys. J.* **609**, 467-473 (2004). doi:10.1086/421103
- S. Matarrese, Relativistic Cosmology: from Superhorizon to Small Scales. in *Dark matter in the universe*, Ed. S. Bonometto, J. R. Primack, A. Provenzale, (IOS Press, Oxford, 1996) pp. 601-628.
- M. V. Medvedev, A. Loeb, Generation of Magnetic Fields in the Relativistic Shock of Gamma-Ray Burst Sources. *Astrophys. J.* **526**, 697-706 (1999). doi:10.1086/308038
- M. V. Medvedev, L. O. Silva, M. Kamionkowski, Cluster magnetic fields from large-scale structure and galaxy cluster shocks. *Astrophys. J. Lett.* **642**, L1-L4 (2006). doi:10.1086/504470
- F. Miniati, A. R. Bell, Resistive magnetic field generation at cosmic dawn. *Astrophys. J.* **729**, id. 73 (2011). doi:10.1088/0004-637X/729/1/73
- P. C. Myers, V. K. Khersonsky, On magnetic turbulence in interstellar clouds. *Astrophys. J.* **442**, 186-196 (1995). doi:10.1086/175434
- D. Nagai, A. Vikhlinin, A. V. Kravtsov, Testing X-ray measurements of galaxy clusters with cosmological simulations. *Astrophys. J.* **655**, 98-108 (2007). doi:10.1086/509868
- A. Neronov, I. Vovk Evidence for strong extragalactic magnetic fields from Fermi observations of TeV Blazars. *Science* **328**, 73-75 (2010). doi:10.1126/science.1184192
- K. I. Nishikawa, J. Niemiec, P. E. Hardee, M. Medvedev, H. Sol, Y. Mizuno, B. Zhang, M. Pohl, M. Oka, D. H. Hartmann, Weibel instability and associated strong fields in a fully three-dimensional simulation of a relativistic shock. *Astrophys. J. Lett.* **698**, L10-L13 (2009). doi:10.1088/0004-637X/698/1/L10
- P. J. E. Peebles, Recombination of the primeval plasma. *Astrophys. J.* **153**, 1-11 (1968). doi:10.1086/149628

- 
- M. V. Penston, Dynamics of self-gravitating gaseous spheres-III. Analytical results in the free-fall of isothermal cases. *Mon. Not. Royal Astron. Soc.* **144**, 425-448 (1969).
- C. Pfrommer, V. Springel, T. A. Enßlin, M. Jubelgas, Detecting shock waves in cosmological smoothed particle hydrodynamics simulations. *Mon. Not. Royal Astron. Soc.* **367**, 113-131 (2006). doi:10.1111/j.1365-2966.2005.09953.x
- C. Pinto, D. Galli, Three-fluid plasmas in star formation. II. Momentum transfer rate coefficients. *Astron. Astrophys.* **484**, 17-28 (2008). doi:10.1051/0004-6361/20078819
- C. Pinto, D. Galli, F. Bacciotti, Three-fluid plasmas in star formation. I. Magneto-hydrodynamic equations. *Astron. Astrophys.* **484**, 1-15 (2008). doi:10.1051/0004-6361/20078818
- R. Plaga, Detecting intergalactic magnetic fields using time delays in pulses of  $\gamma$ -rays. *Nature* **374**, 430-432 (1995). doi:10.1038/374430a0
- R. E. Pudritz, J. Silk, The origin of magnetic fields and primordial stars in protogalaxies. *Astrophys. J.* **342**, 650-659 (1989). doi:10.1086/167625
- I. Røeggen, H. R. Skullerud, T. H. Løvaas, D. K. Dysthe, The  $\text{Li}^+ - \text{H}_2$  system in a rigid-rotor approximation: potential energy surface and transport coefficients. *J. Phys. B* **35**, 1707-1725 (2002). doi:10.1088/0953-4075/35/7/309
- K. Roettiger, J. M. Stone, J. O. Burns, Magnetic field evolution in merging clusters of galaxies. *Astrophys. J.* **518**, 594-602 (1999). doi:10.1086/307298
- D. Ryu, S. Das, H. Kang, Intergalactic magnetic field and arrival direction of ultra-high-energy Protons. *Astrophys. J.* **710**, 1422-1431 (2010). doi:10.1088/0004-637X/710/2/1422
- D. Ryu, H. Kang, Vorticity and turbulence in the large-scale structure of the universe. in *Numerical Modeling of Space Plasma Flows: Astronom 2007*, Ed. N. V. Pogorelov, E. Audit, G. P. Zank, ASP Conference Series **385**, 44-49 (2008).
- D. Ryu, H. Kang, P. L. Biermann, Cosmic magnetic fields in large scale filaments and sheets. *Astron. Astrophys.* **335**, 19-25 (1998).
- D. Ryu, H. Kang, J. Cho, S. Das, Turbulence and magnetic fields in the large-scale structure of the universe. *Science* **320**, 909-912 (2008). doi:10.1126/science.1154923
- D. Ryu, H. Kang, E. Hallman, T. W. Jones, Cosmological shock waves and their role in the large-scale structure of the universe. *Astrophys. J.* **593**, 599-610 (2003). doi:10.1086/376723
- D. Ryu, J. P. Ostriker, H. Kang, R. Cen, A cosmological hydrodynamic code based on the total variation diminishing scheme. *Astrophys. J.* **414**, 1-19 (1993). doi:10.1086/173051
- T. V. Ruzmaikina, A. A. Ruzmaikin, Gravitational stability of an expanding universe in the presence of a magnetic field. *Sov. Astron.* **14**, 963-966 (1971).
- J. I. Sakai, R. Schlickeiser, P. K. Shukla, Simulation studies of magnetic field generation in cosmological plasmas. *Phys. Lett. A* **330**, 384-389 (1999). doi:10.1016/j.physleta.2004.08.007
- A. A. Schekochihin, S. C. Cowley, S. F. Taylor, J. L. Maron, J. C. McWilliams, Simulations of the small-scale turbulent dynamo. *Astrophys. J.* **612**, 276-307 (2004). doi:10.1086/422547
- A. A. Schekochihin, M. Brüggén, L. Feretti, M. W. Kunz, L. Rudnick, Magnetic fields in galaxy clusters: why bother? in this volume (2010).
- D. R. G. Schleicher, R. Banerjee, R. S. Klessen, Reionization: A probe for the stellar population and the physics of the early universe. *Phys. Rev. D* **78**, 083005 (2008). doi:10.1103/PhysRevD.78.083005
- D. R. G. Schleicher, R. Banerjee, S. Sur, T. G. Arshakian, R. S. Klessen, R. Beck, M. Spaans, Small-scale dynamo action during the formation of the first stars and galaxies. I. The ideal MHD limit. *Astron. Astrophys.* , **522**, id. A115 (2010). doi:10.1051/0004-6361/201015184
- D. R. G. Schleicher, D. Galli, S. C. O. Glover, R. Banerjee, F. Palla, R. Schneider, R. S. Klessen, The influence of magnetic fields on the thermodynamics of primordial star formation. *Astrophys. J.* **703**, 1096-1106 (2009). doi:10.1088/0004-637X/703/1/1096

- 
- R. Schlickeiser, P. K. Shukla, Cosmological magnetic field generation by the Weibel instability. *Astrophys. J. Lett.* **599**, L57-L60 (2003). doi:10.1086/381246
- P. Schuecker, A. Finoguenov, F. Miniati, H. Böhringer, H., U. G. Briel, Probing turbulence in the Coma galaxy cluster. *Astron. Astrophys.* **426**, 387-397 (2004). doi:10.1051/0004-6361:20041039
- S. Seager, D. D. Sasselov, D. Scott, A new calculation of the recombination epoch. *Astrophys. J. Lett.* **523**, L1-L5 (1999). doi:10.1086/312250
- S. K. Sethi, B. B. Nath, K. Subramanian, Primordial magnetic fields and formation of molecular hydrogen. *Mon. Not. Royal Astron. Soc.* **387**, 1589-1596 (2008). doi:10.1111/j.1365-2966.2008.13302.x
- S. K. Sethi, K. Subramanian, Primordial magnetic fields in the post-recombination era and early reionization. *Mon. Not. Royal Astron. Soc.* **356**, 778-788 (2005). doi:10.1111/j.1365-2966.2004.08520.x
- J. Silk, M. Langer, On the first generation of stars. *Mon. Not. Royal Astron. Soc.* **371**, 444-450 (2006). doi:10.1111/j.1365-2966.2006.10689.x
- A. G. Sitenko, *Electromagnetic fluctuations in plasma*, Chap. 4 (Academic Press, New York, 1967).
- S. W. Skillman, B. W. O'Shea, E. Hallman, J. O. Burns, M. L. Norman, Cosmological shocks in adaptive mesh refinement simulations and the acceleration of cosmic rays. *Astrophys. J.* **689**, 1063-1077 (2008). doi:10.1086/592496
- R. S. de Souza, R. Opher, Origin of magnetic fields in galaxies. *Phys. Rev. D* **81**, 067301 (2010). doi:10.1103/PhysRevD.81.067301
- K. Subramanian, Unified treatment of small- and large-scale dynamos in helical turbulence. *Phys. Rev. Lett.* **83**, 2957-2960 (1999). doi:10.1103/PhysRevLett.83.2957
- K. Subramanian, J. D. Barrow, Magnetohydrodynamics in the early universe and the damping of nonlinear Alfvén waves. *Phys. Rev. D* **58**, 083502 (1998). doi:10.1103/PhysRevD.58.083502
- K. Subramanian, D. Narashimha, S. M. Chitre, Thermal generation of cosmological seed magnetic fields in ionization fronts. *Mon. Not. Royal Astron. Soc.* **271**, L15-L18 (1994).
- S. Sur, D. R. G. Schleicher, R. Banerjee, C. Federrath, R. S. Klessen, The generation of strong magnetic fields during the formation of the first stars. *Astrophys. J. Lett.* **721**, L134-L138 (2010). doi:10.1088/2041-8205/721/2/L134
- S. I. Syrovatskii, in *Interstellar Gas Dynamics*, ed. H. J. Habing, IAU Symposium No. 39, 192-192 (Springer-Verlag, New York, 1970)
- H. Takami, K. Sato, Distortion of ultra-high-energy sky by galactic magnetic field. *Astrophys. J.* **681**, 1279-1286 (2008). doi:10.1086/588513
- J. C. Tan, E. G. Blackman, Protostellar disk dynamos and hydromagnetic outflows in primordial star formation. *Astrophys. J.* **603**, 401-413 (2004). doi:10.1086/381668
- H. Tashiro, N. Sugiyama, Early reionization with primordial magnetic fields. *Mon. Not. Royal Astron. Soc.* **368**, 965-970 (2006). doi:10.1111/j.1365-2966.2006.10178.x
- The Pierre Auger Collaboration, Correlation of the highest-energy cosmic rays with nearby extragalactic objects. *Science* **318**, 938-943 (2007). doi:10.1126/science.1151124
- R. A. Treumann, R. Nakamura, and W. Baumjohann, Collisionless reconnection: Mechanism of self-ignition in thin plane current homogeneous sheets. *Ann. Geophys.* **28**, 1935-1943 (2010). doi:10.5194/anngeo-28-1935-2010
- C. G. Tsagas, Gravitational waves and cosmic magnetism: a cosmological approach. *Class. Quantum Grav.* **19**, 3709-3722 (2002). doi:10.1088/0264-9381/19/14/311
- C. G. Tsagas, J. D. Barrow, A gauge-invariant analysis of magnetic fields in general-relativistic cosmology. *Class. Quantum Grav.* **14**, 2539-2562 (1997). doi:10.1088/0264-9381/14/9/011
- C. G. Tsagas, R. Maartens, Magnetized cosmological perturbations. *Phys. Rev. D* **61**, 083519 (2000a). doi:10.1103/PhysRevD.61.083519
- C. G. Tsagas, R. Maartens, Cosmological perturbations on a magnetized Bianchi I background. *Class. Quantum Grav.* **17** 2215-2241 (2000b). doi:10.1088/0264-



- 
- 9381/17/11/305
- M. J. Turk, T. Abel, B. O'Shea, The formation of population III binaries from cosmological initial conditions. *Science* **325**, 601-605 (2009). doi:10.1126/science.1173540
- F. Vazza, G. Brunetti, C. Gheller, C., Shock waves in Eulerian cosmological simulations: main properties and acceleration of cosmic rays. *Mon. Not. Royal Astron. Soc.* **395**, 1333-1354 (2009). doi:10.1111/j.1365-2966.2009.14691.x
- C. Vogt, T. Enßlin, A Bayesian view on Faraday rotation maps Seeing the magnetic power spectra in galaxy clusters. *Astron. Astrophys.* **434**, 67-76 (2005). doi:10.1051/0004-6361:20041839
- S. Wang, New primordial-magnetic-field limit from the latest LIGO S5 data. *Phys. Rev. D* **81**, 023002 (2010). doi:10.1103/PhysRevD.81.023002
- I. Wasserman, On the origins of galaxies, galactic angular momenta and galactic magnetic fields. *Astrophys. J.* **224**, 337-343 (1978). doi:10.1086/156381
- E. Weibel, Spontaneously growing transverse waves in a plasma due to anisotropic velocity distribution. *Phys. Rev. Lett.* **2**, 83-84 (1959). doi:10.1103/PhysRevLett.2.83
- L. M. Widrow, Origin of galactic and extragalactic magnetic fields. *Rev. Mod. Phys.* **74**, 775-823 (2002). doi:10.1103/RevModPhys.74.775
- L. M. Widrow, D. Ryu, D. R. G. Schleicher, K. Subramanian, R. A. Treumann, C. Tsagas, The first magnetic fields. in this volume (2010).
- H. Xu, B. W. O'Shea, D. C. Collins, M. L. Norman, H. Li, S. Li, The Biermann battery in cosmological MHD simulations of population III star formation. *Astrophys. J. Lett.* **688**, L57-L60 (2008). doi:10.1086/595617
- Y. Xu, P. P. Kronberg, S. Habib, Q. W. Dufton, A Faraday rotation search for magnetic fields in large-scale structure. *Astrophys. J.* **637**, 19-26 (2006). doi:10.1086/498336
- N. Yoshida, K. Omukai, L. Hernquist, Protostar formation in the early universe. *Science* **321**, 669-671 (2008). doi:10.1126/science.1160259
- Y. B. Zeldovich, The Hypothesis of Cosmological Magnetic Inhomogeneity. *Sov. Astron.* **13**, 608-611 (1970a).
- Y. B. Zeldovich, Separation of uniform matter into parts under the action of gravitation. *Astrofizika* **6**, 319-335 (1970b).
- Y. B. Zeldovich, V. G. Kurt, R. A. Sunyaev, Recombination of hydrogen in the hot model of the universe. *Sov. Phys. JETP* **28**, 146-150 (1969).
- Y. B. Zeldovich, A. A. Ruzmaikina, D. D. Sokolov, *Magnetic fields in astrophysics* (Gordon and Breach Science Publishers, New York, 1983).